PERFORMANCE OF HYBRID AND PURE ANALOG CSI FEEDBACK IN MIMO SYSTEMS WITH TIME-SELECTIVE FADING

by

Phoenix Yuan
B.A.Sc. (Computer Engineering), Simon Fraser University, 2007

THESIS SUBMITTED IN PARTIAL FULFILLMENT OF
THE REQUIREMENTS FOR THE DEGREE OF

MASTER OF APPLIED SCIENCE

In the
School of Engineering Science

SIMON FRASER UNIVERSITY

Spring 2010

APPROVAL

Name: **Phoenix Yuan**

Degree: **Master of Applied Science**

Title of Thesis: **Performance of Hybrid and Pure Analog CSI Feedback in MIMO Systems with Time-Selective Fading**

Examining Committee:

Chair: **Dr. Stephen Hardy**
Professor of the School of Engineering Science

Dr. Paul Ho
Senior Supervisor
Professor of the School of Engineering Science

Dr. Jie Liang
Supervisor
Assistant Professor of the School of Engineering Science

Dr. Sami Muhaidat
Internal Examiner
Assistant Professor of the School of Engineering Science

Date Defended/Approved: Mar-1-2010

Declaration of
Partial Copyright Licence

ABSTRACT

In a Frequency division duplex (FDD) system, knowledge of channel state information (CSI) at the transmitter requires a closed feedback loop. In this thesis, we examine system performance associated with different types of feedback operating in time-selective Rayleigh fading channels. For a singleuser system with multiple transmit antennas, we consider hybrid analog/digital feedback, which is an extension for the traditional digital-only codebook feedback. An extra analog symbol that encapsulates channel's amplitude and phase information that is otherwise lost in the codebook quantization process is fed back for channel tracking purpose. For a multiuser multiple-input-multiple-output (MIMO) system, we consider the deployment of pure analog CSI feedback. A modified minimum mean square error (MMSE) criterion is used to incorporate downlink channel prediction into the precoder design and user selection process. In both cases, the proposed types of CSI feedback can achieve better BER in comparison to digital CSI feedback.

Keywords: wireless communication; CSI feedback; analog feedback; hybrid feedback; MMSE precoding; MIMO

ACKNOWLEDGEMENTS

I am forever indebted to my senior supervisor, Dr. Paul Ho, for his guidance and encouragement. Special thanks are due to Dr. Sami Muhaidat and Dr. Jie Liang for examining and reviewing this thesis, and to Dr. Stephen Hardy for chairing my thesis defence. I would like to thank SFU for hosting such a pleasant working environment filled with great teachers and wonderful friends.

In addition, I would like to express my gratitude for my family. They provide years of care, encouragement, and support throughout my studies.

TABLE OF CONTENTS

LIST OF FIGURES

LIST OF TABLES

GLOSSARY

AWGN	Additive white Gaussian noise
BER	Bit error rate
CSI	Channel State Information
DD	Differential detection
FDD	Frequency division duplex
MISO	Multiple-input-single-output
MIMO	Multiple-input-multiple-output
MRC	Maximal ratio combining
MMSE	Minimum mean square error
MSE	Mean square error
MU	Multi-user user
PU2RC	Per-user unitary rate control
SINR	Signal-to-interference-plus-noise ratio
SNR	Signal-to-noise ratio
SQRC	Square root raised cosine
TDD	Time division duplex
iid	Independent and identically distributed
pdf	Probability density function

NOTATIONS

$E[\cdot]$	Expectation operator
$J_0(\cdot)$	Zero-th order Bessel function of the first kind
$\mathrm{Re}\{\cdot\}$	Real part of a complex number
$\mathrm{Im}\{\cdot\}$	Imaginary part of a complex number
$\Pr\{\cdot\}$	Probability of an event
$diag(a_1, a_2, \ldots, a_N)$	Diagonal matrix containing $a_1, a_2, \ldots, a_N$
$(\cdot)^H$	Hermitian transpose
$(\cdot)^T$	Matrix transpose

CHAPTER 1 INTRODUCTION

In wireless communication, the environment surrounding a transmitter and receiver can affect the traversing signal. Due to presence of reflectors, the receiver will pick up multiple copies of the same transmitted signal. Each copy experienced different attenuation, delay and phase shift, resulting in a phenomenon termed multipath fading. When the interference from fading is destructive, the communication channel experienced a severe drop in quality. As a result, the weaken signal will experienced significant increase in transmission error. In order to achieve a more reliable reception, system designers can utilize diversity technique. By deploying multiple antennas at the transmitter and/or at the receiver, proper use of signal processing techniques can mitigate the fading effect in wireless channel.

We focus on personal mobile communication system where the transmitter is a base station equipped with multiple antenna and the receivers are single-antenna mobile units. In such system, beamforming can achieve transmit diversity by manipulating the transmitted signals from different antennas in a way that causes the channel fading to combine constructively at the receiver. In order to compute the beamformer, the transmitter requires knowledge of sufficiently accurate channel state information (CSI). In a time division duplex (TDD) system, the reciprocal principle dictates the uplink and downlink CSI in the same

frequency band to be identical. Therefore, the base station can acquire CSI through direct sampling of the uplink channel. In contrast, a frequency division duplex (FDD) system uses different frequency bands for uplink and downlink channels. Therefore, the base station has to obtain certain information from the mobile through a closed-loop feedback uplink. The feedback information conveyed some notion of the downlink channel condition, whether it is in the form of channel state, interference level, receiver power, etc. The base station can then use this information to adapt downlink transmission.

In this thesis, we explore different feedback strategies for multi-antenna, FDD closed-loop systems. Our focus is on systems operating in a fast fading environment, where exploiting the temporal correlation in the fading channels can result in improved system performance. Two CSI-related topics are presented. For a singleuser Multiple-Input-Single-Output (MISO) system, we propose a novel analog/digital hybrid CSI feedback method. Additionally, we investigate the effectiveness of using analog feedback in a multi-user Multiple-Input-Multiple-Output (MIMO) system. The results are verified by computer simulation. We start by reviewing some of the contributions in these research areas.

1.1 Codebook-based Digital Feedback

To overcome the challenge of making instantaneous channel adaptation, a base station requires periodic feedback from mobile(s). Codebook-based digital feedback system has already gain supported in 3GPP LTE, IEEE 802.16, and

other next-generation wireless system. In most cases, the codebook is computed off-line and stored in both the transmitter and the receiver. Therefore, the receiver only needs to feedback the preferable index of codebook matrix or vector.

Codebook design and utilization is still a hot research topic. The existing design strategies include differential codebook [1] [2] [3], non-unitary codebook [4], adaptive codebook [5], partitioned codebook [6], etc. For independent and identically distributed (i.i.d) channel, codebook design based on complex Grassmannian line packing, such as the ones used in the IEEE 802.16 standard, is considered optimal [7]. However, the Grassmannian codebook does not address the correlation that exists in a more realistic channel condition. In response, the codebook design in [8] [9] takes channel spatial correlation into consideration. Similarly, in [5] temporal correlation in the channel is utilized to create the adaptive codebook. However, its design procedure requires real-time knowledge of channel parameters at both the transmitter and the receiver, which is a rather difficult goal in practice. Therefore, we are motivated to investigate practical adaptive codebook scheme that requires minimum feedback overhead.

1.2 Closed-Loop Multi-user MIMO

Multi-user MIMO broadcast channel can increase system multiplexing gain through simultaneous mobile transmission. This technique, known as space-division multiple access (SDMA), can achieve higher throughput compare to

other multiple-access scheme such as time-division multiple access (TDMA) [10]. The optimal SDMA strategy, known as dirty paper coding (DPC) [11], is non-casual and difficult to realize. Practical alternatives are the minimum mean-square error (MMSE) precoding scheme in [12] [13] [14] and the unitary precoding scheme in [15] [16]. Furthermore, their performance can be enhanced through multi-user diversity, where the base station only transmits to a carefully selected subset of users that have strong channels. Another precoding approach is zero-forcing beamforming (ZFBF) [17], where the precoder is set to the pseudo-inverse of the channel matrix. While this precoder forces the multi-user interference to zero, unfortunately the transmission power suffers when the channel matrix is near singular. In contrast, the MMSE precoder allows some mutual interference between users in exchange for better performance, especially at low signal-to-noise (SNR) region.

In order for the base station to compute the MMSE precoder, the mobile terminals need to feedback the estimated downlink CSI periodically. The accuracy of CSI is found to have a large impact on performance [14] [17] [18] [19] [20] [21]. Traditionally, the CSI, or its derivatives, is first quantized and then fed back to the base station. We will refer to this approach as digital/quantized feedback. It has been found in [22] that for single-user transmit beamforming systems operating in a fast fading environment, digital feedback is substantially worse than the so-called analog feedback approach, whereby the measured channel gains are fed back in their original form without any quantization. The

effectiveness of deploying analog feedback for a multi-user MIMO system subjected to fast fading has yet to be considered.

It should be noted that although analog feedback transmission requires high dynamic range, the issue has been studied and addressed in [23]. The solution is to apply a pre-determined power-clipping threshold to limit peak power. It has been found in [23] that imposing a constraint on analog symbols' instantaneous power has little impact on overall performance.

1.3 Thesis Outline

The thesis is structured in the following manner. Chapter 2 presents the signal and system model that well be used throughout the thesis. The basic downlink and uplink closed-loop feedback framework are established in this chapter.

Chapter 3 covers a singleuser MISO beamforming system that uses codebook-based digital feedback. We introduce an adaptive codebook design based on analog/digital hybrid feedback information. The proposed scheme has very little overhead, and can be easily adopted into existing digital feedback-only codebook framework such as the one in IEEE 802.16. Performance results for the new feedback scheme operating in fast fading channels are shown and benchmarked.

In Chapter 4, we expand the scope of the system into a multi-user MIMO scheme. Similar to [23] (which studies a singleuser MISO system), we compare

the performance of MMSE precoder designed using analog and digital CSI feedback. We also present a multi-user scheduling algorithm that can account for the temporal correlation in user channels. Included in this chapter is an alternative precoder design based on unitary codebook. It is used as a reference to demonstrate the robustness of MMSE precoder operating in fast fading channels.

Finally, the last chapter summarizes the work in this thesis and provides suggestion for related future work in this area.

1.4 Contributions of this Thesis

We investigated two main topics in the thesis. First, we noted that a common drawback for most of the codebook-based limited feedback scheme is they do not account for temporal channel correlation. Therefore, we present a novel hybrid-feedback scheme to enhance the robustness of a MISO beamforming system. At the cost of slight increase in feedback throughput, the new scheme is able to convert a fixed codebook into an adaptive codebook that matches the instantaneous realization of the channel, resulting in improved BER performance in a fast fading environment.

Second, we examine the use of analog feedback for multi-user MIMO system. Although the optimal MMSE precoder design has already been demonstrated in [13], the use of MMSE criterion for user scheduling has not been established. We present a MSE based user selection algorithm that determines

the users set based on the feedback CSI. The MMSE precoding user selection find the optimal set of users by calculating the mean square error (MSE) between the precoder and the predicted channel response. We demonstrate the importance of channel tracking by showing that unitary precoding system performs poorly in time-selective channels.

CHAPTER 2 BACKGROUND

In this chapter, we establish the underlying models and conventions for the MIMO and MISO communication systems. A brief description of baseband signal representation is covered in Section 2.1. MISO and MIMO downlink transmission framework is reviewed in Section 2.2. The uplink SIMO feedback framework is established in Section 2.3. Section 2.4 discusses downlink and uplink channel estimation. Section 2.5 covers channel linear prediction. Finally, simulation conventions are the subject of Section 2.6. A brief chapter summary is provided in Section 2.7.

2.1 Baseband Representation of Bandpass Systems

In digital communication, data is sent by modulating a carrier with an information signal, whose bandwidth is typically much smaller than the carrier frequency. The resulting modulated signals are termed narrowband bandpass signals. They can be expressed in the form

$$\begin{aligned}\tilde{s}(t) &= A(t)\cos(2\pi f_c t + \theta(t)) \\ &= \mathrm{Re}\{s(t)e^{j2\pi f_c t}\}\end{aligned} \qquad \textbf{(2.1.1)}$$

where $A(t)$ and $\theta(t)$ are respectively the amplitude and phase of the information signal; f_c is the carrier frequency; $s(t) = A(t)e^{j\theta(t)}$ is the complex baseband

equivalent of the bandpass signal $\tilde{s}(t)$; For the sake of mathematical convenience, we represent the modulated signals and channels by their baseband equivalents. For this reason, the complex baseband representation is used in the rest of this thesis. Therefore, without any loss of generality, we are only concerned with the transmission of the equivalent low-pass signal through the low-pass channels.

2.2 Downlink Transmission model

In this thesis, we are concerned with the downlink data transmission from a base station equipped with L transmit antennas to one or multiple mobile units equipped with a single receive antenna. For downlink transmission, the system model is either single-user MISO or multi-user MIMO.

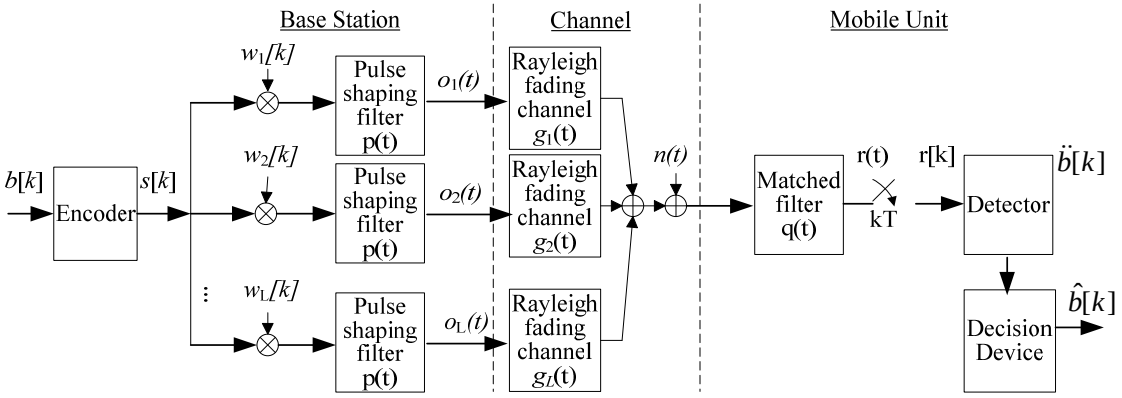

Figure 2.2-1 Downlink MISO transmission model.

2.2.1 Single-user MISO Model

The general MISO structure is depicted in Figure 2.2-1. At discrete time k, binary data are Gray-mapped into a $M-ary$ PSK data symbol $b[k]$ drawn from the set $\left\{e^{j2\pi c/M}; c=0,1,\ldots,M-1\right\}$. Either the data symbol is transmitted directly as $s[k]=b[k]$, or it is encoded differentially as $s[k]=b[k]s[k-1]$, where $s[k-1]$ is the encoded symbol at discrete time $k-1$. The encoded symbol $s[k]$ is then replicated across the L antennas, and weighted by the beamforming vector $\mathbf{w}[k]$ to form the transmitted signal vector $\mathbf{o}[k]$ as

$$\mathbf{o}[k]=\begin{bmatrix} o_1[k] \\ o_2[k] \\ \ldots \\ o_L[k] \end{bmatrix}=\begin{bmatrix} w_1[k] & 0 & \ldots & 0 \\ 0 & w_2[k] & \ldots & 0 \\ \ldots & \ldots & \ldots & \ldots \\ 0 & 0 & 0 & w_L[k] \end{bmatrix}\begin{bmatrix} s[k] \\ s[k] \\ \ldots \\ s[k] \end{bmatrix} \quad \textbf{(2.2.1)}$$

A unity energy square root raised cosine (SQRC) pulse shaping filter $p(t)$ is used to modulate $o_l[k]$. The resulting transmitted signal over the *l*-th antenna is

$$o_l(t)=\sum_k t_l[k]\,p(t-kT), \quad \textbf{(2.2.2)}$$

where $1/T$ is the baud rate. The transmitted signal is sent through a frequency-nonselective Rayleigh fading channel with additive white Gaussian noise (AWGN). As depicted in Figure 2.2-1, the wireless channel introduced fading patterns $g_l(t)$, $l=1,2,\ldots,L$, and AWGN component $n(t)$. We assume there exist

sufficient separation between the L base station antennas, such that the channel gains $g_l(t)$, $l = 1, 2, \ldots, L$, are independent and identically distributed (i.i.d). Moreover, the channel gain $g_l(t)$ is a zero mean complex Gaussian random process with variance $\sigma_g^2 = \frac{1}{2} E\left[\left| g_l(t) \right|^2 \right]$. A Rayleigh isotropic scattering channel model is assumed, resulting in the well-known U-shaped Jakes fading spectrum with a Jakes autocorrelation

$$\varphi_g(\tau) = \frac{1}{2} E\left[g_l(t)\, g_l^*(t-\tau) \right] = \sigma_g^2 J_0(2\pi f_d \tau), \qquad \textbf{(2.2.3)}$$

where $J_0(\cdot)$ is the operator for the zero-th order Bessel function of the first kind, and f_d is the Doppler frequency. The noise term $n(t)$ is a complex white Gaussian random process with zero mean and a unity power spectral density.

At the receiver, the received signal $r(t)$ is filtered by a SQRC matched filter $q(t) = p(-t)$. The output is sampled at $t = kT$, and therefore the received symbol is

$$r[k] = \begin{bmatrix} g_1[k] & g_2[k] & \ldots & g_L[k] \end{bmatrix} \begin{bmatrix} o_1[k] \\ o_2[k] \\ \ldots \\ o_L[k] \end{bmatrix} + n[k], \qquad (2.2.4)$$

where $g_l[k]$, $o_l[k]$, $n_l[k]$ are respectively the sampled version of $g_l(t)$, $o_l(t)$, and $n(t)$. It can be shown that the sampled channel gain $g_l[k]$ has an autocorrelation function of

$$\varphi_g[d] = \frac{1}{2} E\left[g_l[k]^* g_l[k-d] \right] = \sigma_g^2 J_0\left(2\pi d f_d T\right). \quad \textbf{(2.2.5)}$$

The beamforming vector $\mathbf{w}[k]$ that generates transmitted signal vector $\mathbf{o}[k]$ is designed to influence the received symbol $r[k]$. It does so by aligning the phases of the individual components in the fading vector $\mathbf{g}[k]$ such that the power of the composite signal is maximized. Construction of the beamformer $\mathbf{w}[k]$ will be further explored in Chapter 3. Because of this phase alignment, the receiver can choose to perform coherent detection if it wants. In this case, the transmitted symbols are $s[k] = b[k]$ and the received symbol $r[k]$ can be used directly as the decision variable, $\ddot{b}[k] = r[k]$. On the other hand, if differential encoding is used instead, then $r[k]$ is subjected to differential detection, $\ddot{b}[k] = r[k] r^*[k-1]$. Finally, the estimated data symbol is recovered from $\ddot{b}[k]$ via the following decision device

$$\tilde{b}[k] = \begin{cases} 0, & \ddot{b}[k] \le 0 \\ 1, & \ddot{b}[k] > 0 \end{cases} \quad \textbf{(2.2.6)}$$

2.2.2 Multi-user MIMO Model

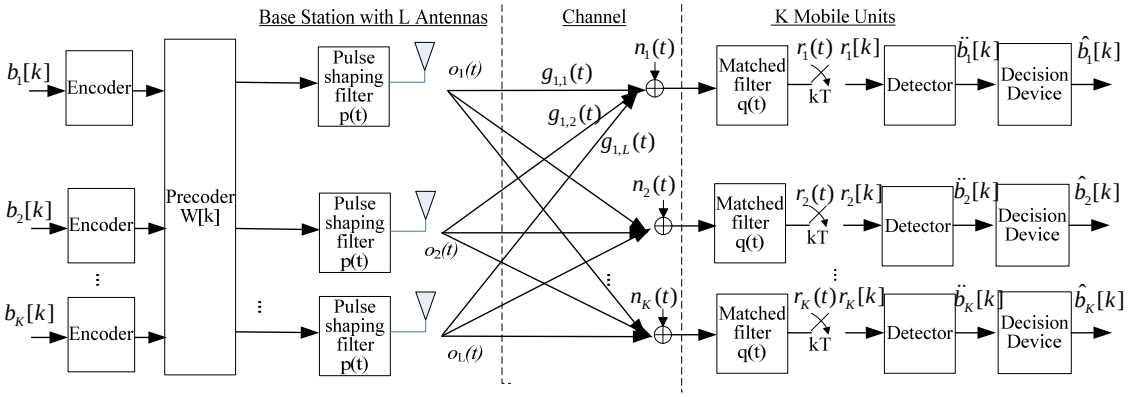

Figure 2.2-2 Downlink MISO transmission model.

Figure 2.2-2 shows the general Multi-user MIMO structure. It is similar to the MISO model in Section 2.2.1, with the exception that Z independent data streams are simultaneously transmitted to Z mobile units. The size of the user pool is M, therefore the base station is responsible for selecting Z out of M users for active data transmission. At discrete time k the base station transmits the symbol

$$\mathbf{o}[k]=\begin{bmatrix} o_1[k] \\ o_2[k] \\ \dots \\ o_L[k] \end{bmatrix}=\begin{bmatrix} \mathbf{w}_1[k] & \mathbf{w}_2[k] & \dots & \mathbf{w}_K[k] \end{bmatrix}^T \begin{bmatrix} s_1[k] \\ s_2[k] \\ \dots \\ s_K[k] \end{bmatrix} \qquad \textbf{(2.2.7)}$$

where $\mathbf{w}_l[k]=\begin{bmatrix} w_{l,1}[k] & w_{l,2}[k] & \dots & w_{l,K}[k] \end{bmatrix}^T$ forms the beamforming vector for user l. Collectively, $\mathbf{W}[k]=\begin{bmatrix} \mathbf{w}_1[k] & \mathbf{w}_2[k] & \dots & \mathbf{w}_K[k] \end{bmatrix}^T$ is the precoder at discrete time k. For an active user l, its received signal is

$$
\begin{aligned}
r_l[k] &= \begin{bmatrix} g_{1,l}[k] & g_{2,l}[k] & \ldots & g_{L,l}[k] \end{bmatrix} \begin{bmatrix} o_1[k] \\ o_2[k] \\ \ldots \\ o_L[k] \end{bmatrix} + n_l[k] \\
&= \left(\sum_{a=1}^{L} g_{a,l}[k] o_a[k] \right) + n_l[k] \qquad , \qquad \textbf{(2.2.8)} \\
&= \left(\sum_{a=1}^{L} g_{a,l}[k] \mathbf{w}_a^T[k] \mathbf{s}[k] \right) + n_l[k] \\
&= \mathbf{g}_l[k] \mathbf{w}_l[k] s_l[k] + \left(\sum_{a=1, a \neq l}^{L} \mathbf{g}_l[k] \mathbf{w}_a[k] s_a[k] \right) + n_l[k]
\end{aligned}
$$

where $\mathbf{s}[k] = \begin{bmatrix} s_1[k] & s_2[k] & \ldots & s_K[k] \end{bmatrix}^T$. Using the detection and decoding procedures described in Section 2.2.1, $r_l[k]$ provides sufficient information to recover the $l-th$ data symbol estimated $\tilde{b}_l[k]$.

Multi-user MIMO is considered more complicated than single-user MISO, since the precoder $\mathbf{W}[\mathrm{k}]$ serve two objectives. The first objective is that the precoder should provide a beamforming effect, just like its counterpart in the MISO system. Secondly, as shown in (2.2.8), there are two non-noise components in user $l's$ received signal. The first term in (2.2.8) is the desired signal term for user l, while the second term is the sum of all the interference terms from the data streams of the other the $Z-1$ users. Therefore, the precoder is also responsible for suppressing multi-user interference. Ideally, the precoder should amplify the power of the first term for all users; simultaneously, it minimizes the power of the interference term. This is a non-trivial task since signal power for one user becomes an interference term to all another users.

Chapter 4 will further elaborate precoder design and multi-user selection base on the MMSE criterion.

2.3 Uplink Transmission model

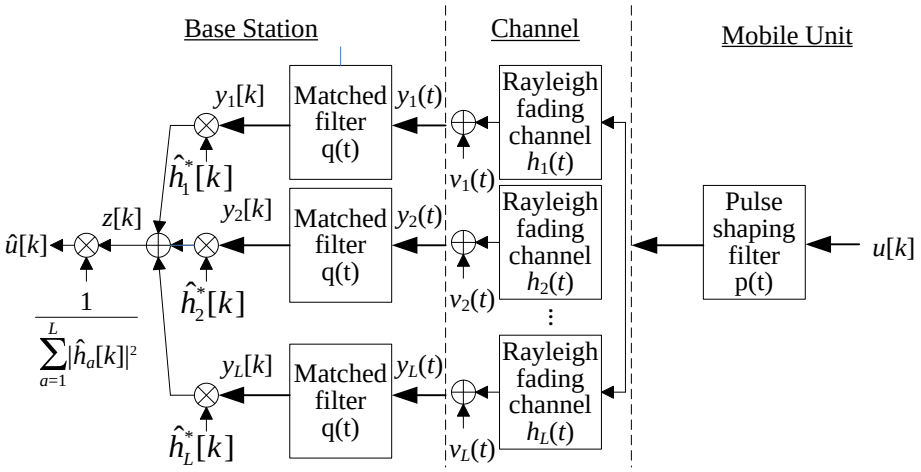

Figure 2.3-1 Uplink SIMO transmission model.

In order to design the beamformer or the precoder, the base station requires knowledge of channel condition via the mobile unit(s)' feedback uplink. As Figure 2.3-1 shows, uplink transmission is formulated as a SIMO framework that consists of a single mobile antenna and L base station antennas. For a single-user system, the mobile feedbacks CSI symbol $u[k]$ to the base station in the form of $u(t)=\sum_k u[k]p(t-kT)$, where $p(t)$ is a unit-energy SQRC pulse. The feedback signal $u(t)$ arrives at the base station over L frequency-nonselective Rayleigh fading channels as

$$y_l(t) = h_l(t)u(t) + v_l(t),\ l = 1, 2, ..., L\text{,} \qquad \textbf{(2.3.1)}$$

where $h_l(t)$ is the uplink channel gain and $v_l(t)$ is the noise term of the $l-th$ channel. The channel gain $h_l(t)$ is a complex Gaussian random process with zero mean, variance $\sigma_h^2 = \frac{1}{2}E\left[\left|h(t)\right|^2\right]$, and a Jakes autocorrelation

$$\varphi_h(\tau) = \frac{1}{2}E\left[h(t)h^*(t-\tau)\right] = \sigma_h^2 J_0(2\pi f_d \tau)\text{.} \qquad \textbf{(2.3.2)}$$

On the other hand, the noise term $v_l(t)$ is a zero mean complex white Gaussian random process with a power spectral density of unity. The fading gains $h_l(t), l = 1, 2, ..., L$ and noise term $v_l(t), l = 1, 2, ..., L$ from different base station antennas are assumed i.i.d.

The base station matched filters the received signals $y_l(t), l = 1, 2, ..., L$ and samples the filter output at $t = kT$. Therefore the received symbol is

$$y_l[k] = h_l[k]u[k] + v_l[k],\ l = 1, 2, ..., L \qquad \textbf{(2.3.3)}$$

where $y_l[k]$, $h_l[k]$, $u[k]$, $v_l[k]$ are the sampled version of their counterparts in the continuous domain. The sampled channel gain $h_l[k]$ has an autocorrelation function of

$$\varphi_h[d] = \frac{1}{2} E\left[h[k]^* h[k-d] \right] = \sigma_h^2 J_0\left(2\pi d f_d T\right), \quad \textbf{(2.3.4)}$$

and the noise term $v_l[k]$ has variance $\sigma_v^2 = 1$. In order for the base station to recover the CSI data from each antenna, it must first remove the uplink fading gain. For each uplink channel l, assuming the fading gain estimate $\hat{h}_l[k]$ is obtained, the fading effect can be removed by first performing maximal ratio combining (MRC) and then divide the result by the summed fading energy as follows:

$$\begin{aligned} \hat{u}[k] &= \frac{\sum_{l=1}^{L} \hat{h}_l^*[k] y_l[k]}{\sum_{l=1}^{L} \left|\hat{h}_l[k]\right|^2} \\ &= \frac{\sum_{l=1}^{L} \hat{h}_l^*[k](\hat{h}_l[k]u[k] + v_l[k])}{\sum_{l=1}^{L} \left|\hat{h}_l[k]\right|^2}. \\ &= u[k] + \frac{v_l[k]}{\sum_{l=1}^{L} \left|\hat{h}_l[k]\right|^2} \end{aligned} \quad \textbf{(2.3.5)}$$

The uplink framework in a multi-user is similar to the one for single-user, except the CSI information from different users must be transmit at the same time. Frequency division multiple access (FDMA) will be used in the dedicated uplink to prevent mutual interferences. Given that the per-user symbol rate in the dedicated uplink is the same as that in the downlink data channel, the uplink's bandwidth will be M times that of the downlink. Fortunately, the frame structure in the uplink enables it to be shared by multiple base stations through TDMA.

This combination of FDMA and TDMA for the uplink ensures only a moderate level of CSI overhead is required per base-station per frame.

2.4 Channel Estimation

Based on the described transmission models, both the base station and the mobile unit(s) are required to perform periodical channel estimation to mitigate channel fading. In the downlink, since the transmitted symbols from different base station antennas are detected by the mobile unit as a single composite symbol, a simple orthogonal pilot sequences is adopted to ensure channel separation. As shown in Figure 2.4-1, each antenna sends a L-symbol-long pilot sequence, with $\mathbf{p}_1 = [1\,0\,0 \ldots 0]$, $\mathbf{p}_2 = [0\,1\,0 \ldots 0\,0]$, ..., $\mathbf{p}_L = [0\,0 \ldots 0\,1]$. These pilot patterns imply that during the pilot transmission phase, only a single antenna is activated at each symbol duration. Consequently, there is no mutual interference between different antennas during channel estimation.

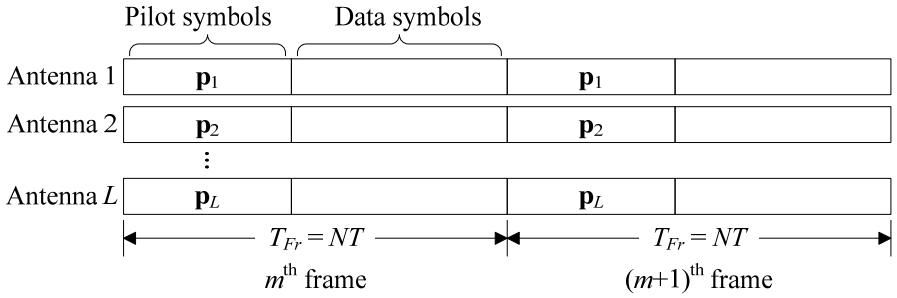

Figure 2.4-1 Downlink data frame structure.

We adopt a general downlink frame structure that occupies N symbols. L symbols are used as pilots and the remaining $F = N - L$ symbols are allocated for data transmission. Symbol duration is denoted as T and every frame spans $T_{frame} = TN$ seconds. According to the Nyquist sampling criterion, the pilot frame rate is constrained by $1/T_{frame} \geq 2 f_d$, since the channel gains have a bandwidth equal to the Doppler frequency f_d.

For the m-th frame, let the $l-th$ channel's downlink gains during pilot transmission be represented by the diagonal matrix

$$\mathbf{G}[m] = diag\left(g_l[mN], g_l[mN+1], \ldots, g_l\left[mN+(L-1)\right]\right), l = 1, 2, \ldots, L, \quad \textbf{(2.4.1)}$$

the mobile unit can obtain the estimates of the L downlink gains correspond to the non-zero pilot symbols as

$$\begin{aligned} \hat{g}_l[mN+(l-1)] &= r[mN+(l-1)] \\ &= \mathbf{p}_l \mathbf{G}_l[m] + n[mN+(l-1)] \\ &= g_l[mN+(l-1)] + n[mN+(l-1)] \\ & \qquad l = 1, 2, \ldots L \end{aligned}, \quad \textbf{(2.4.2)}$$

The downlink gain estimates $\hat{g}_l[mN+(l-1)], l = 1, 2, \ldots, L$ have zero mean and variance of $\sigma_{\hat{g}}^2 = \sigma_g^2 + \sigma_n^2$. These channel estimates, in its current or digitized form, must be feedback from each mobile to the base-station. This forms the C CSI symbols $u[k], k = mN, mN+1, \ldots mN+(C-1)$ in (2.3.5). As shown in Figure 2.4-2, the structure of the feedback uplink frame is similar to the downlink frame,

with the exception that only a single unit-magnitude pilot symbol is required for every T_{frame} seconds. For the $m-th$ frame, the pilot symbol received by l-th base station antenna is $y_l[mN] = h_l[mN]P + v_l[mN]$, where $P = 1$ is the uplink pilot symbol. Therefore, the channel gain estimate for the m-th uplink frame is

$$\begin{aligned} \hat{h}_l[mN] &= y_l[mN] \\ &= h_l[mN] + v_l[mN] \end{aligned}, \qquad \textbf{(2.4.3)}$$

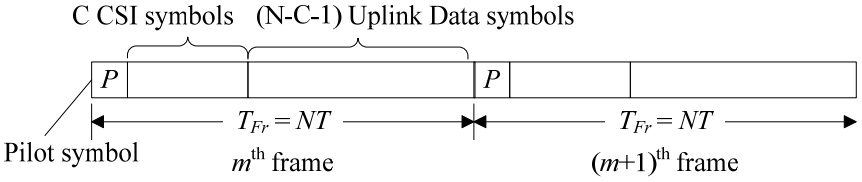

Figure 2.4-2 Uplink data frame structure.

2.5 Channel Prediction

As we had shown in Section 2.4, pilot symbol is used to perform periodic channel estimation. Specifically, for every T_{frame} seconds, or every N symbols, the base station emits pilot sequences to all the mobiles; similarly, a pilot symbol is inserted into every uplink frame to facilitate CSI feedback transmission.

For the $m-th$ frame, the uplink pilot symbols enable the system to obtain channel estimates $\hat{h}[mN]$ (2.4.4). Based on this channel estimate and a collection of past pilot estimates, the base station can use linear prediction to extrapolate fading gain estimate that affect the C CSI symbol positions of the

$m-th$ frame, $\hat{h}[mN+l-1], l=1,2,...,C$ ('CSI symbols' in Figure 2.4-2). The linearly predicted fading gains are critical for the CSI recovery equation in (2.3.5).

Suppose a $J-th$ order predictor is used for linear prediction, channel gain estimates $\hat{h}[mN+f]$ at the f data position is given by

$$\hat{h}[mN+f] = \mathbf{c}[f]\mathbf{r}, \tag{2.5.1}$$

where $\mathbf{c}[f] = \left[c^{(J-1)}[f] \quad c^{(J-2)}[f] \quad ... \quad c^{0}[f] \right]$ are the filter coefficients and

$\mathbf{r} = \left[\hat{h}\left[(m-J+1)N\right] \quad \hat{h}\left[(m-J+2)N\right] \quad ... \quad \hat{h}\left[(mN\right] \right]^{T}$ is the vector that contains the J most recently obtained uplink pilot estimates. The reason why the filter is only a function of the timing phase, f, of the symbol, rather than absolute time, k, is because of the stationary assumption in the fading and noise processes.

The optimal coefficients $\mathbf{c}[f]$ is determined by the Weiner filter, which is optimal in the mean square sense,

$$\begin{aligned} \varepsilon^2[f] &= \frac{1}{2} E[\left| h[mN+f] - \hat{h}[mN+f] \right|^2] \\ &= \frac{1}{2} E[\left| h[mN+f] - \mathbf{c}[f]\mathbf{r} \right|^2] \\ &= \sigma_h^2 + \mathbf{c}[f]\mathbf{\Phi}_{rr}\mathbf{c}^{\dagger}[f] - \mathbf{\Phi}_{hr}[f]\mathbf{c}^{\dagger}[f] - \mathbf{c}[f]\mathbf{\Phi}_{rh}[f] \end{aligned} \quad , \tag{2.5.2}$$

where $\mathbf{\Phi}_{rr} = \frac{1}{2} E[\mathbf{r}\mathbf{r}^H]$ is the autocorrelation matrix of the past channel gains $\mathbf{r}$, and $\mathbf{\Phi}_{hr}[f] = \frac{1}{2} E\left[\hat{h}[mN+f]\mathbf{r}^H \right] = \mathbf{\Phi}_{rh}^{\dagger}[f]$ is the cross-correlation vector between

$\hat{h}[mN+f]$ and $\mathbf{r}$. By solving $\frac{\partial}{\partial \mathbf{c}[f]}\varepsilon^2[f]=0$, the coefficients are determined according to

$$c[f]=\mathbf{\Phi}_{hr}[f]\mathbf{\Phi}_{rr}^{-1} \tag{2.5.3}$$

The uplink channel distribution follows the Jakes model, therefore the correlation $\mathbf{\Phi}_{rr}$ and $\mathbf{\Phi}_{hr}[f]$ are the same among all channels. The autocorrelation matrix for the pilot estimates $\mathbf{\Phi}_{rr}$ is

$$\begin{aligned}\mathbf{\Phi}_{rr} &= \frac{1}{2}E[\mathbf{r}\mathbf{r}^H] \\ &= \frac{1}{2}E\left[\begin{pmatrix}\hat{h}_{(m-j+1)N}\\ \hat{h}_{(m-j+2)N}\\ \cdots\\ \hat{h}_{mN}\end{pmatrix}\begin{pmatrix}\hat{h}_{(m-j+1)N} & \hat{h}_{(m-j+2)N} & \cdots & \hat{h}_{mN}\end{pmatrix}\right],\end{aligned} \tag{2.5.4}$$

where the $(i,j)-th$ element of $\mathbf{\Phi}_{rr}$ matrix, $0\le i,j\le J$ is

$$\begin{aligned}\mathbf{\Phi}_{rr}(i,j) &= \frac{1}{2}E[\hat{h}_i\hat{h}_j^*] \\ &= \begin{cases}\sigma_h^2+\sigma_v^2, & if\ i=j\\ \sigma_h^2 J_0(2\pi f_d(i-j)T), & otherwise\end{cases}\end{aligned} \tag{2.5.5}$$

Similarly, the cross-correlation function $\mathbf{\Phi}_{hr}[f]$ between $\hat{h}[\mathrm{mN}+\mathrm{f}]$, and the past pilot estimates $\mathbf{r}$ is

$$\mathbf{\Phi}_{hr}[f] = \frac{1}{2} E[\hat{h}[mN+f]\mathbf{r}^*]$$
$$= \left[\sigma_h^2 J_0(2\pi f_d fT) \quad \sigma_h^2 J_0(2\pi f_d (f-mN)T) \quad \ldots \quad \sigma_h^2 J_0(2\pi f_d (f-(J-1)mN)T) \right]^T \quad \textbf{(2.5.6)}$$

The corresponding MSE of the gain estimated obtained through linear prediction is

$$\varepsilon^2[f] = \sigma_h^2 = \mathbf{\Phi}_{hr}[f]\mathbf{\Phi}_{rr}^{-1}\mathbf{\Phi}_{rh}[f] \quad \textbf{(2.5.7)}$$

As we shall explain in the subsequent chapters, if the CSI is analog feedback, scalar quantized digital feedback, or hybrid feedback, then the base station can extract downlink channel gain information from the CSI. In these instances, a second layer of linear prediction can combat fast fading during downlink data transmission. Suppose the base station obtains downlink channel gain estimates $\tilde{g}_l[mN+(l-1)],\ l=0,1,...,L-1$, then the downlink gain $\tilde{g}_l[mN+(L-1)+f]$ at the f data symbol position can be estimated by

$$\tilde{g}_l\left[mN+(L-1)+f\right] = \mathbf{e}_l\left[f\right]\mathbf{d}_l,\ l=1,2,\ldots,L, \quad \textbf{(2.5.8)}$$

where $\mathbf{e}_l\left[f\right] = \left[e_l^{(J-1)}\left[f\right] e_l^{(J-2)}\left[f\right] \ldots e_l^{(0)}\left[f\right] \right]$ are the filter coefficients and

$$\mathbf{d}_l = \left[\tilde{g}_l\left[\left(m-J+1\right)N+\left(l-1\right)\right] \quad \tilde{g}_l\left[\left(m-J+2\right)N+\left(l-1\right)\right] \quad \ldots \quad \tilde{g}_l\left[mN+\left(l-1\right)\right] \right]^T$$

are the J most recent downlink gain estimates obtained through the feedback uplink.

Similar to (2.5.3), the correlation coefficients $\mathbf{e}_l[k]$ are given by

$$\mathbf{e}_l[f] = \mathbf{\Phi}_{gd,l}[f]\mathbf{\Phi}_{dd,l}^{-1} \quad \textbf{(2.5.9)}$$

However, deriving the correlation $\mathbf{\Phi}_{gd,l}[f]$ and $\mathbf{\Phi}_{dd,l}$ are much less straightforward than their uplink counterparts. The reason is that while uplink PSAM is effective in mitigating uplink fading gains, the recovered downlink channel estimates $\tilde{g}_l[mN+(l-1)],\ l=0,1,...,L-1$ are still subjected to residue uplink noise and PSAM MSE (2.5.7). Moreover, uplink CSI can adopt one of several quantized forms, which further complicates the formulation of the downlink channel correlation. For simplicity, we assume $\mathbf{\Phi}_{gd,l}[f]$ and $\mathbf{\Phi}_{dd,l}$ are known priori through sampling the actual downlink channel and then correlate the data directly to the feedback CSI. Also, as noted in [23], the received signals have a phase error diffuse component once the second layer of prediction is applied. For this reason, we adopt differential encoding and differential detection in our simulation.

2.6 Simulation Conventions

Throughout this thesis, performance results obtained by computer simulations will use the conventions defined in this section.

2.6.1 Power Convention

Transmission error rate is the BER averaged over the F data positions in the downlink frames. BER result is plotted against downlink SNR given as

$$\gamma = \left(\frac{N}{F}\right)\left(\frac{\sigma_g^2}{\sigma_n^2}\right), \tag{2.6.1}$$

where the first factor accounts for the loss in transmission efficiency due to the pilot symbol and the second term is the raw link-SNR. In essence, the raw SNR is the received SNR when neither precoding nor beamforming is used at all, i.e. the base station devotes all the power to one antenna and transmits to only one user. Downlink transmission power per antenna is σ_g^2 / L. To equalize antenna power consumption, uplink transmission power per antenna is set to $\sigma_h^2 = \sigma_g^2 / L$.

2.6.2 Feedback Delay

For the sake of simplicity, we chose not to inject feedback delay into the previous background sections. But in a more practical system model, transmission and processing time create a feedback delay that must be taken into account. As is the case in [23], the minimal delay, denoted as D, is equal to or greater than the number of feedback symbols C. As shown in Figure 2.6-1, after the base station sends out the pilot sequence, there is a $T_{feedback} = DT$ seconds delay before it receives all the CSI from the mobile.

Figure 2.6-2 shows the effect of delay on downlink data transmission. In essence, transmission of the $m-th$ data block begins only after the base station obtains all the corresponding CSI feedback. Linear prediction of downlink fading gains has to be extended by $L+D$ symbols, where L of the fading gain estimates at the $(m+1)-th$ frame's pilot symbol positions will not be used. As feedback delay increases, the filter has to predict further into the future, and therefore prediction error is expected to increase.

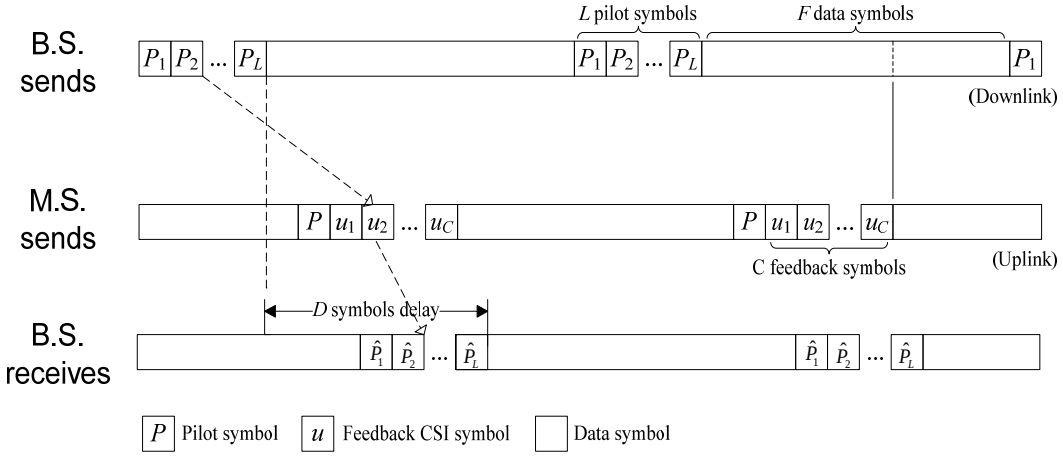

Figure 2.6-1 Delay in feedback uplink.

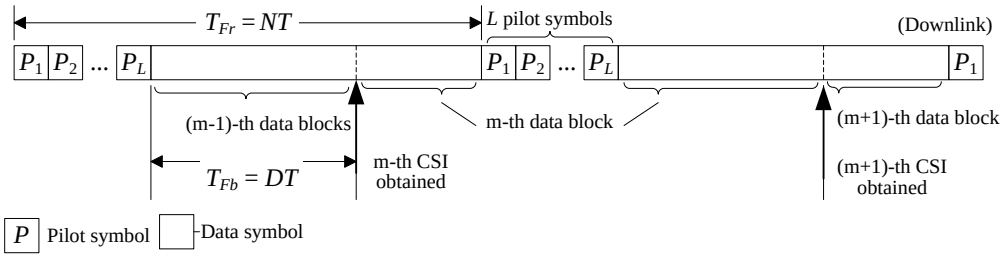

Figure 2.6-2 Effect of delay on downlink transmission.

2.6.3 Channel Convention

We had emphasized that the targeted mobile environment is modelled as time-selective Rayleigh fading with Jakes distribution. In the simulation, we will also show the performance result when the system operates in a static Rayleigh fading environment, where fading is modelled as white complex Gaussian process with zero mean and unity variance. In essence, the normalized Doppler frequency $f_d T$ becomes zero and both uplink and downlink channels remain constant across an entire frame. It can be shown that in block fading, the PSAM Wiener filter used in the downlink and uplink are degenerated to simple time-averaging filters.

2.7 Summary

This chapter establishes the signal and system models that will be use throughout the subsequent chapters. We described the single-user MISO and multi-user MIMO transmission framework. In downlink transmission, data signal is manipulated by transmission weight, which is computed using CSI obtained from the uplink channel. The base station uses MRC to achieve full receive-diversity. The mobile and the base station both perform periodic channel estimation. Furthermore, the base station can utilize two layers of linear predictions to combat time-selective fading in the uplink and downlink channels. In the next two chapters, we shift our focus to the different CSI feedback

schemes, as well as various different beamformer or precoder design and comparison.

CHAPTER 3 PROPOSED HYBRID FEEDBACK FOR SINGLEUSER MISO SYSTEMS

In closed-loop transmit beamforming, transmit diversity is achieved through the coordination of signal directionality from the different antennas. The technique is adaptive in nature, in which the base station has to obtain downlink channel knowledge from the mobile via feedback signaling. The periodical feedback information is then used to calculate the optimal transmit weight such that the received SNR is maximized. The effectiveness of transmit beamforming is highly dependent on the accuracy of the feedback information.

Codebook-based digital feedback has been adopted into many next-generation wireless standards. A drawback we identified in the traditional fixed-codebook feedback is that it is not compatible with the linear prediction scheme presented in Section 2.5. We shall demonstrate that this problem can be solved using a new analog/digital hybrid feedback scheme. Consequently, the hybrid feedback approach affords improved performance in the presence of fast fading.

This chapter contains the following sections. The existing fixed codebook beamforming system is introduced in Section 3.1 as the reference. The hybrid feedback scheme is presented in Section 3.2. CSI Implementation issue is the subject in Section 3.3. Computer simulation and the results are shown in Section 3.4. Finally, the chapter is summarized in Section 3.5.

3.1 Fixed Codebook MISO Beamforming

We considered the MISO system introduced in Section 2.2, where there are L antennas at the transmitter and a single antenna at the receiver. The system uses transmitter beamforming to mitigate the channel fading effect. A closed feedback loop is used to transmit CSI from the receiver to the transmitter. The beamforming vector $\mathbf{w}$ employed by the transmitter is chosen from a fixed unitary codebook $\mathbf{V}$ that is shared by the receiver and the transmitter. The entries in the codebook, $\mathbf{v}_1, \mathbf{v}_2, ..., \mathbf{v}_{2^B}$, are vectors of size $L \times 1$, and if the $i-th$ vector $\mathbf{v}_i$ is selected, then the B bits binary code associated with $\mathbf{v}_i$ will be fed back to the base station over the uplink.

Let $\boldsymbol{g} = (g_1, g_2, ..., g_L)$ be the vector of downlink channel gains and n be the zero-mean additive white Gaussian noise (AWGN) term affecting the unit-energy pilot symbol s. Then the received signal sample, after using $\mathbf{w}$ as the beamformer, is

$$r = \mathbf{g}\mathbf{w}s + n. \qquad \textbf{(3.1.1)}$$

As noted in Section 2.4, the mobile obtains channel estimation via pilot symbol. Therefore, only an estimate $\hat{\boldsymbol{g}} = (\hat{g}_1, \hat{g}_2, ..., \hat{g}_l)$ is available at the mobile, instead of the true gain $\boldsymbol{g}$. The receiver's perception of (3.1.1) becomes $r = \hat{\mathbf{g}}\mathbf{w}s + n$. It thus searches for the "best" vector from the set $\{\mathbf{v}_1, \mathbf{v}_2, ..., \mathbf{v}_{2^B}\}$ that maximizes the perceived signal-to-noise ratio (SNR) in r

$$SNR_r = \frac{\left|\hat{\mathbf{g}}\mathbf{w}\right|^2}{\sigma_n^2} \qquad \textbf{(3.1.2)}$$

where σ_n^2 is the variance of the noise term *n* in (3.1.1). As a result, the receiver sets

$$\mathbf{w} = \arg\max_{i=1,2,...,2^B} \left|\hat{\mathbf{g}}\mathbf{v}_i\right|^2 \qquad \textbf{(3.1.3)}$$

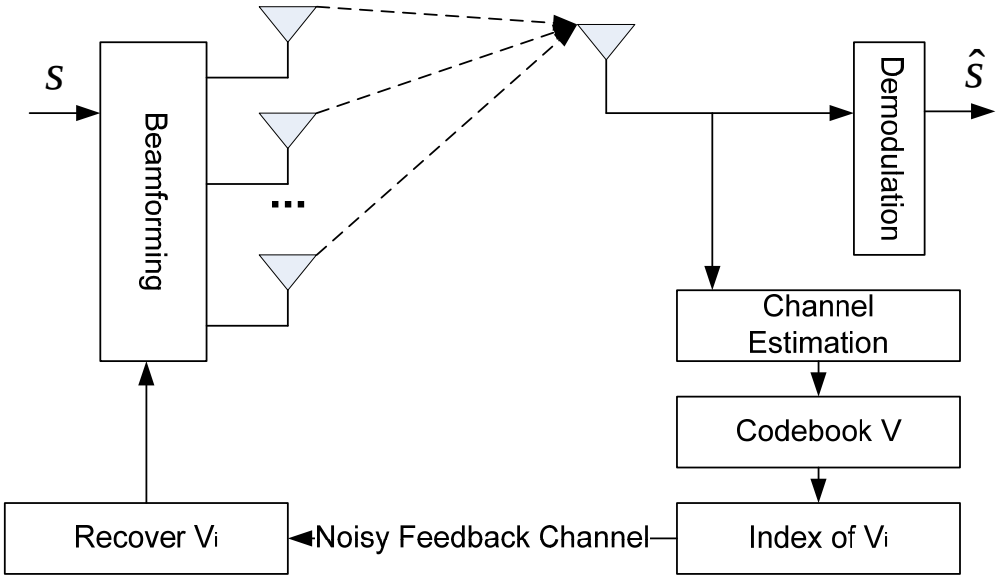

Figure 3.1-1 Fixed-codebook feedback for MISO systems.

Since the codebook is unitary, $\left|\mathbf{v}_i\right|^2 = 1$ for all $i = 1, 2, ..., 2^B$, the transmitter does not have to perform any power scaling no matter which codeword is selected. Upon receiving the code vector index from the uplink, the base station transmitter will use the corresponding code vector as the beamformer. As a reminder, the feedback uplink we adopted is non-ideal; hence, the recovered

index is not guaranteed to be the one intended. The operations used for fixed codebook feedback are summarized in Figure 3.1-1.

3.2 Hybrid extension

The unitary codebooks we mentioned in the last section are taken from [24] and the relevant information is reproduced in Appendix 1. As observed from (A.7), these codebooks have the characteristics that the first entry in every code vector is always a non-negative real quantity, i.e. zero-phase. In essence, the receiver uses the first antenna as a phase reference. While this approach reduces the number of code vectors needed and hence decreases the feedback rate, it limits the signal detection option to differential detection. Furthermore, since the codebook is unitary, the amplitude information in the channel gains is also lost. The lost of both amplitude and phase information prevents the use of linear predictive beamforming to compensate for time-selective fading in the channel. As a result, the performance of the digital-only feedback scheme in the last section can be quite disappointing in such an operating environment [22]. In this section, we introduce a hybrid feedback approach whereby an additional analog feedback symbol is used to provide the amplitude and phase references required in linear-predictive beamforming. The inclusion of this analog feedback symbol also opens up the possibility for coherent detection.

Consider first the beamformer selection in (3.1.3) under the assumption of an infinitely large codebook of unit vectors, i.e. $B \to \infty$. In this case, the selected beamformer will, intuitively, assume the form of $\mathbf{w}_\infty = e^{j\theta_1}\hat{\mathbf{g}}^* / \left\|\hat{\mathbf{g}}^*\right\|$, where

$$\theta_1 = \arg\left\{\hat{g}_1\right\} \tag{3.2.1}$$

is the phase of the estimated channel gain $\hat{g}_1$, and $(\cdot)^*$ denotes element-wise conjugation of a matrix. The phase angle in (3.2.1) is used to ensure that the phase of the other antennas are measured against the phase of the first antenna. With a finite codebook though, the selected beamformer will be a quantized version of $\mathbf{w}_\infty$. In other words, except for the amplitude scaling and phase shifting that are involved, beamformer selection is equivalently to quantization of $\hat{\mathbf{g}}^*$. Since the statistics of $\hat{\mathbf{g}}^*$ and the gain vector $\hat{\mathbf{g}}$ are identical, one quickly realizes that the same codebook can be used for quantization of $\hat{\mathbf{g}}$ directly. In this case, the receiver selects directly the code vector $\mathbf{v}$ from the codebook that is closest to $\hat{\mathbf{g}}^T$, i.e.

$$\mathbf{v} = \arg\min_{i=1,2,\ldots,2^B} \left\| \frac{\hat{\mathbf{g}}^T}{a} - \mathbf{v}_i \right\|^2 = \arg\min_{i=1,2,\ldots,2^B} \left\{ \mathrm{Re}\left[\hat{\mathbf{g}}^T \mathbf{v}_i^H e^{-j\theta_1} \right] \right\}, \tag{3.2.2}$$

where

$$a = \left\|\hat{\mathbf{g}}\right\| e^{j\theta_1} . \qquad \textbf{(3.2.3)}$$

Note that the division of $\hat{\mathbf{g}}^T$ by a in (3.2.2) is needed due to the unitary nature of the codewords and because the first element of each codeword is real and non-negative. The same factor, however, has no impact on beamformer selection in (3.1.3), as it will have the same effect on all the code vectors.

Once $\mathbf{v}$ is determined according to (3.2.2), its binary code will be fed back to the base-station via the uplink. The transmitter can simply use $\mathbf{w} = \mathbf{v}^*$ as the beamformer[1]. However, the resultant close-loop system is then not much different from the pure digital feedback scheme described in the last section, except for the way the beamformer is selected. Consequently, it will experience the same problems: no possibility for coherent detection and predictive beamforming. In this investigation, we advocate a hybrid approach whereby the scalar a in (3.2.3) is sent as an extra analog feedback symbol, along with the digital modulation symbols associated with $\mathbf{v}$. Upon receiving both $\mathbf{v}$ and a, the base station obtain an estimate of $\hat{\mathbf{g}}^T$ according to

$$\tilde{\mathbf{g}}^T = a\mathbf{v} \qquad \textbf{(3.2.4)}$$

It should be pointed out that because of the quantization error in $\mathbf{v}$, $\tilde{\mathbf{g}}^T$ will not be identical to $\hat{\mathbf{g}}^T$, even if there is no feedback error. However, with a sufficiently

[1] This is only true if the base station does not perform any further downlink channel prediction based on $\mathbf{v}$. If it does, then the beamformer $\mathbf{w}$ for each data symbol is simply the conjugate of the result of this second layer of channel prediction; see Section 2.5.

large codebook, the quantization error will become insignificant when compared to other channel impairments.

The proposed hybrid approach increases the effective resolution of the codebook through exploiting and feeding back the complex symbol a. Alternatively speaking, it turns the original fixed codebook into an adaptive codebook according to the value of a. The beauty here is that the increased resolution is achieved without the need to make any change to the codebook. The amplitude and phase of a provide sufficient information for the base station to restore the magnitude and phase of individual components of $\tilde{\mathbf{g}}^T$. This means the base station can now use a collection of past gain vectors $\tilde{\mathbf{g}}^T$'s it obtains for the pilot phases in successive frames to predict the channel gains that affect the data symbols, leading to a linear-predictive beamforming system that can be used to combat fast fading. Furthermore, the technique opens up the possibility of coherent detection at the receiver because the phase of the product term $\mathbf{gw}$, $\mathbf{w} = \mathbf{v}^*$, in (3.1.1) will only wiggle slightly around zero phase. In conclusion, the two major problems associated with the pure digital feedback approach can be mitigated with this new hybrid approach. We summarize in Figure 3.2-1 the system model of this feedback scheme.

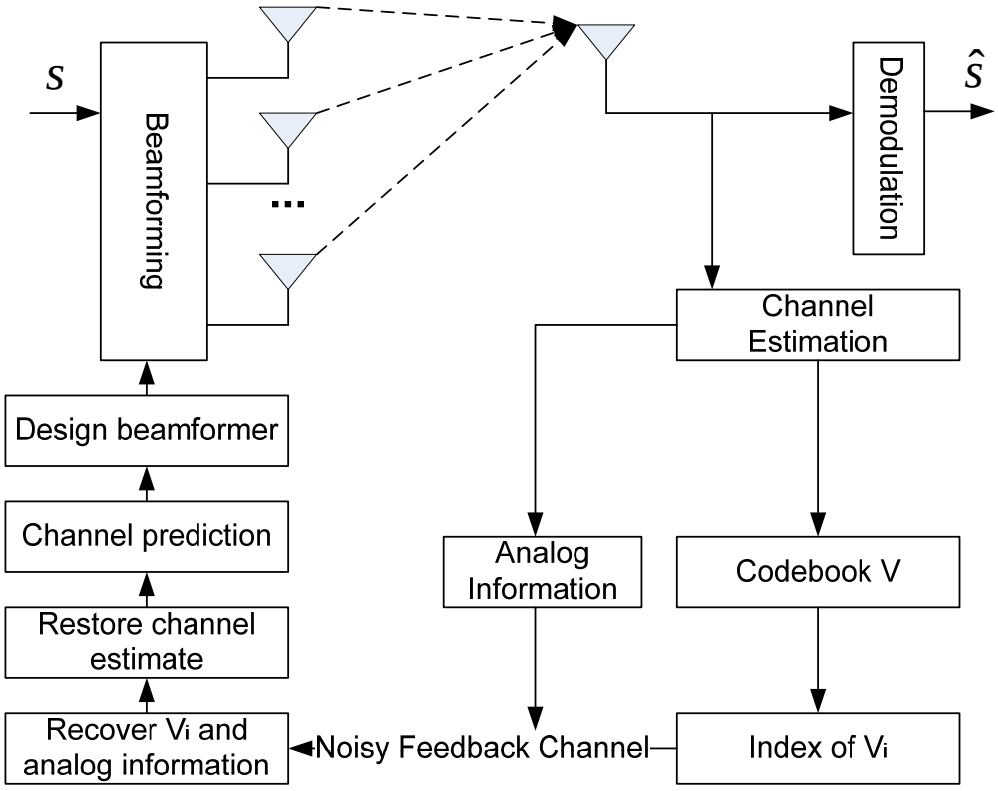

Figure 3.2-1 Hybrid codebook feedback for MISO system.

3.3 Implementation Issue

Recalling from Section 2.4 how the receiver obtains the downlink channel estimates $\hat{g}_l,\ l=1,2,...,L$ during the pilot transmission phase of a frame. These channel estimates are then forwarded to the unitary codebook. Depending on the feedback approach, either (3.1.3) or (3.2.2) will be used. The codebook index will be converted into C *M*-ary PSK (MPSK) symbols, where $C\log_2 M$ is the number of bits used to represent the codebook indices. In the case of the hybrid feedback scheme, the analog symbol a in (3.2.3) is computed and transmitted along with the MPSK symbols over the uplink.

In the uplink, PSAM described in Section 2.5 will be used to send C or $C+1$ CSI symbols to the base station. The feedback symbols will arrive at the transmitter after a delay of DT seconds. A soft estimate of any CSI symbol u is obtained according (2.3.5). If u is an MPSK symbol, a hard decision will be made and the bit pattern obtained from all such decisions will be used to select $\hat{\mathbf{v}}$ from the codebook as the most likely feedback code vector. In the case that u is the analog CSI symbol in (3.2.3), then no hard decision will be made and $\hat{u}$ will simply be used as the estimate of a. This estimate will be denoted as $\hat{a}$. We remind the reader that due to error introduced in the feedback link, $\hat{\mathbf{v}} \neq \mathbf{v}$ and $\hat{a} \neq a$ in general.

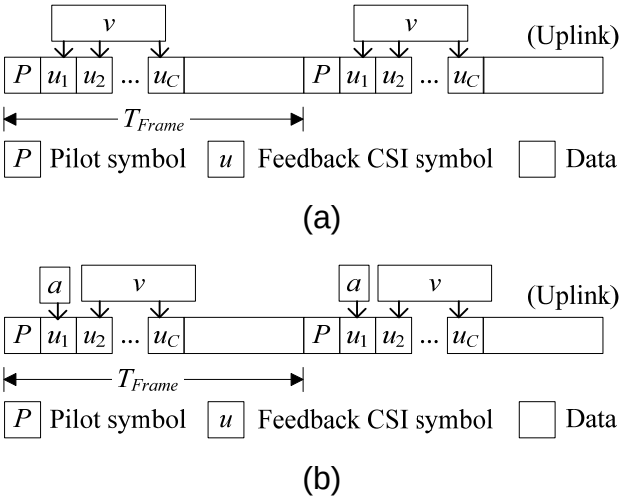

Figure 3.3-1 (a) Codebook CSI feedback; (b) Hybrid CSI feedback

As a reminder, the frame structure we adopted is shown in Figure 3.3-1. Recall that the rationale of proposing the hybrid feedback approach is that it

enables the base station to perform linear-predictive beamforming in a time-selective fading environment. Let $(\hat{\mathbf{v}}[m], \hat{a}[m])$, $m = 0,1,..., J-1$, be the codewords and analog CSI symbols recovered by the base station for Frame 0 to Frame $J-1$. Without loss of generality, we assume frame m starts at time mNT and ends at time $m(N+1)T$. For each pair of $(\hat{\mathbf{v}}[m], \hat{a}[m])$ in the hybrid scheme, the base station constructs the channel gain estimate for the pilot phase of that frame according to

$$\tilde{\mathbf{g}}^T[m] = \hat{a}[m]\hat{\mathbf{v}}[m], \qquad \textbf{(3.3.1)}$$

where the k-th element in $\tilde{\mathbf{g}}^T[m]$ is an estimate of the path gain $g_k(t)$ affecting the pilot symbols in the n-th downlink frame. From $\tilde{\mathbf{g}}^T[m]$, $m = 0,1,..., J-1$, the fading gains affecting each data symbol in the $J-$th frame can be estimated through linear prediction described in Section 2.5. Once the gain vector $\tilde{\mathbf{g}}$ at a data position is obtained, it will be converted to a beamformer through the operation

$$\mathbf{w} = \tilde{\mathbf{g}}^* / \left\| \tilde{\mathbf{g}}^* \right\| . \qquad \textbf{(3.3.2)}$$

Another alternative is

$$\mathbf{w} = \tilde{\mathbf{g}}^{*} / \sqrt{E\left[\tilde{\mathbf{g}}\tilde{\mathbf{g}}^{H}\right]} \ . \qquad \textbf{(3.3.3)}$$

Both options will satisfy the unit power constraint. In (3.3.2), the vector norm is used to normalize the power of the beamforming vector to unity; the norm needs to be calculated for every beamforming vector. In (3.3.3), the beamforming vector is normalized by the ensemble average of $\tilde{\mathbf{g}}$ instead; the ensemble average only needs to be calculated once offline. Simulation results show that the difference in performance between the two power normalization schemes is minimal[2]. Therefore, in this investigation, we only adopt (3.3.2). In summary, with the availability of the analog CSI symbol, linear predictive beamforming can be realized. The base station can now vary the beamformer from symbol to symbol according to the instantaneous channel condition.

Finally, let us consider a detail implementation issue when the channel exhibits block fading. In this situation, assuming absence of pilot estimation error, all the feedback $(\mathbf{v}[m], a[m])$'s are identical, but the received $(\hat{\mathbf{v}}[m], \hat{a}[m])$'s at the base station are not because of uplink imperfection. Intuitively, we can use an averaging filter to mitigate this imperfection in the uplink. The filter simply uses

[2] The authors in [13] also make the same observation regarding beamformer power normalization

$$\tilde{\mathbf{g}}^T = \frac{1}{J}\sum_{m=0}^{J-1} \hat{a}[m]\hat{\mathbf{v}}[m] \qquad \textbf{(3.3.4)}$$

as an estimate of $\hat{\mathbf{g}}^T$. Yet another possibility is based on the majority decision, $\hat{\mathbf{v}}_{maj}$, of the received code vectors $\hat{\mathbf{v}}[m]$:

$$\tilde{\mathbf{g}}^T = \bar{\hat{a}} \cdot \hat{\mathbf{v}}_{maj}, \qquad \textbf{(3.3.5)}$$

where $\bar{\hat{a}}$ is the average of a subset of $\hat{a}[m], m = 0,1,...,J-1;\ \hat{a}[i]$ belongs to this subset if $\hat{\mathbf{v}}[i] = \hat{\mathbf{v}}_{maj}$, that is, only analog symbol paired with the majority code vector are used in the mean calculation of a. We will refer to this last case as the majority decision approach. In both cases, $\tilde{\mathbf{g}}^T$ is not necessarily a code vector of the codebook. It should be pointed out (3.3.4) and (3.3.5) can be modified for the pure digital feedback approach described in Section 3.2 by simply replacing the $\hat{a}[m]$'s or $\bar{\hat{a}}$ with unity.

3.4 Result and Discussion

We present in this section the simulation results for the proposed hybrid feedback scheme. For the purpose of illustration, we consider simulations defined by the parameters listed in Table A. We assume the base station is equipped with 3 or 4 antennas. Each downlink frame consists of $F = 80$ differential BPSK (DBPSK) (± 1) data symbols; for beamforming purposes, $J = 10$ order predictors are used at the base-station to predict the downlink gains based

on the quantized CSI. Both data downlinks and CSI feedback uplinks are Rayleigh fading channels. In the time-selective fading scenario, we assume a normalized Doppler frequency of $f_d T = 0.002$ and $f_d T = 0.005$. This corresponds to a vehicle speed of 35 km/hr and 85 km/hr for a carrier frequency of 1.9 GHz and a 30 KHz baud rate. Unless otherwise stated, there is no feedback delay. The codebooks used are defined in Appendix 1. It is assumed that the mobile modulates the 6-bits codebook index into 3 QPSK symbols, and therefore there are a total of 3 CSI symbols for digital feedback and 4 CSI symbols for hybrid feedback.

Table A Simulation parameters.

Base antennas L	Channel Type	Normalized Doppler frequency $f_d T$	Channel coherence time $1/f_d$	Channel estimation rate (approx.) $1/T_{Fr}$, $T_{Fr} = NT$	Frame size N
4	Fast fading	0.002	$500T$	$6 f_d$	84
		0.005	$200T$	$2.5 f_d$	
3	Fast fading	0.002	$500T$	$6 f_d$	83
		0.005	$200T$	$2.5 f_d$	
4	Block Fading	N/A			84
3	Block fading				83

We adopt these naming conventions for the BER curves: (a) curves labelled as digital feedback is based on the beamformer design described in Section 3.1; see (3.1.3). Curves labelled as hybrid feedback is based on the quantizer approach with analog side information described in Section 3.2; see (3.2.2) and (3.3.2); (b) For simulation in block fading environment, we found that the averaging filter performs best for hybrid feedback, while majority decision works best for digital feedback. Unless stated otherwise, the use of average filter in hybrid feedback and the use of majority decision in digital feedback in block fading simulation are implicit.

Figure 3.4-1 shows the BER performance for a 4 antennas system with different filtering options operating in a block-fading environment. Without the averaging or the majority decision device to reduce estimation error at the transmitter, the performances of the two feedback schemes are identical[3]. The difference is that in the hybrid feedback scheme, the magnitude and phase of the channel can be estimated from the analog feedback symbol. In turns of throughput, the original digital-only scheme has the advantage, since it requires one less feedback symbol. The performance of the two schemes is no longer identical once the averaging and the majority decision device are included in the system. At BER of 10^{-3}, the hybrid (quantizer) approach receives roughly a 6 dB gain in power efficiency when compared to no averaging, while the gain for the pure digital (beamformer) method is 4.5 dB with majority decision device. Using

[3] This is equivalent to using a first order predictor based on $(\hat{\mathbf{w}}[Q], \hat{a}[Q])$

the averaging filter for the digital method actually deteriorates the BER performance. As explained in Section 3.2, the beamformers chosen by (3.1.3) does not retain the phase information of the downlink pilot estimate, and therefore these codebook vectors cannot be summed directly.

In Figure 3.4-2 to Figure 3.4-4, we show the performance curves for 4 antennas and 3 antennas systems with different normalized Doppler frequency. In all scenarios, hybrid feedback has superior performance in comparison to digital feedback. The largest performance gain occurs in a block-fading environment, where both 3 antennas and 4 antennas systems achieve a 2 dB gain at BER of 10^{-3}. As expected, time-variation in the channel has a significant effect on the BER. Comparing to the block fading results in Figure 3.4-2, the fast fading results in Figure 3.4-3 shows a 6 dB drop in power efficiency at a BER of 10^{-3} for the 4-antenna hybrid feedback system. Figure 3.4-3 shows that at high SNR and a normalized Doppler frequency of 0.002, hybrid feedback is roughly 1 dB to 2 dB more efficient than digital feedback. When Doppler frequency is increased to 0.005, as shown in Figure 3.4-4, the advantage of using hybrid feedback increases to a gain of 2dB. This result is expected, since without the channel phase information, digital feedback cannot utilize linear prediction to adapt the selected beamformer. Consequently, its performance degrades more rapidly as channel variation increases. The opposite is true for hybrid feedback, whose use of linear prediction enables some compensation against the correlated time variation in the channel.

The results also suggest that increasing channel variation reduces the multi-antenna diversity effect. With no channel variation, a 4 antennas system is roughly 3dB more power efficient than a 3 antennas system, as shown in Figure 3.4-2. The gap is significantly narrowed in Figure 3.4-3, and it all but disappeared in Figure 3.4-4.

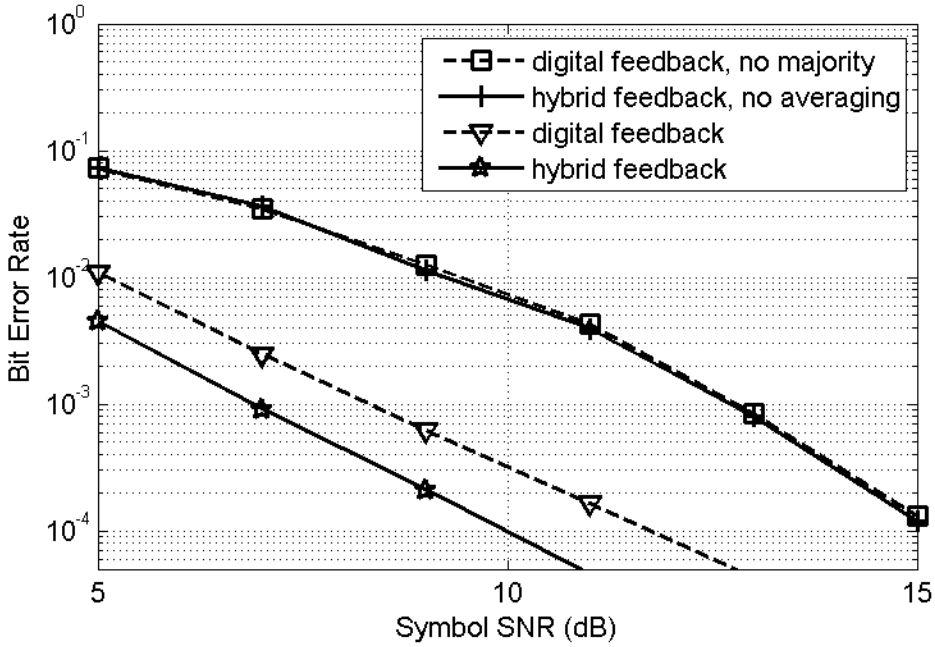

Figure 3.4-1 BER of hybrid and digital feedback in block fading channel; Different uplink filtering options; 4 antennas

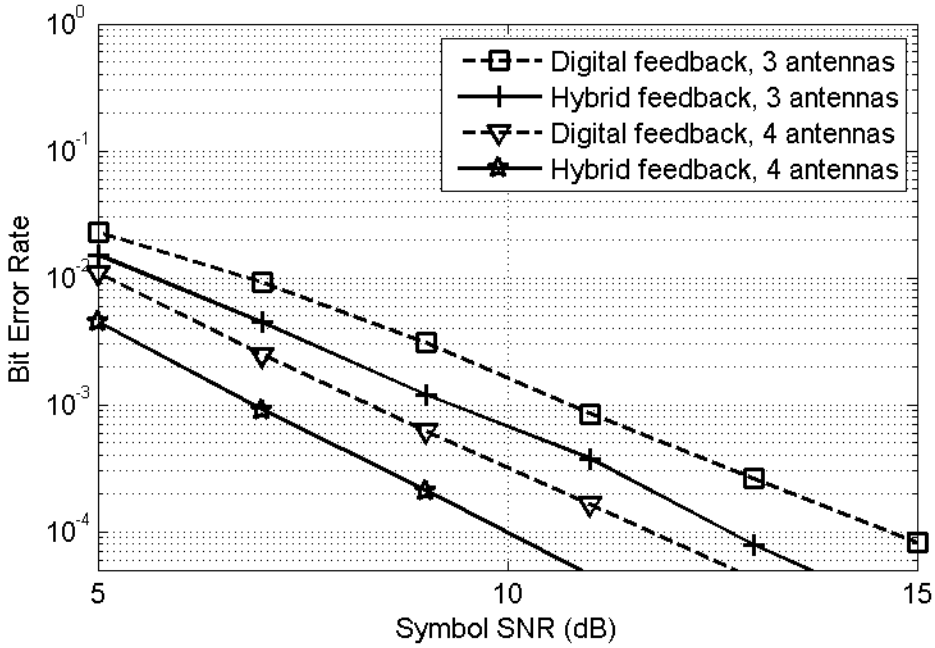

Figure 3.4-2 BER of hybrid and digital feedback in block fading channel.

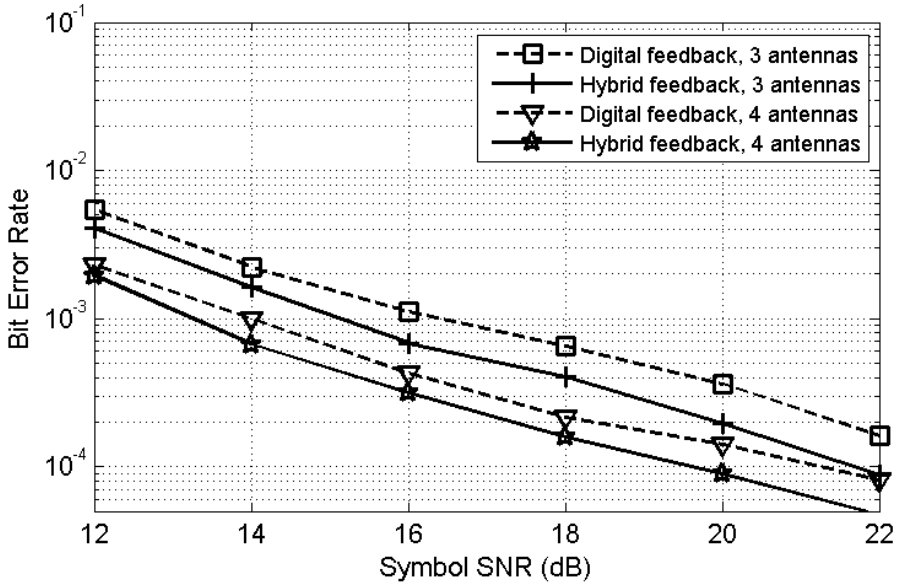

Figure 3.4-3 BER of hybrid and digital feedback in fast fading channel; $f_d T = 0.002$.

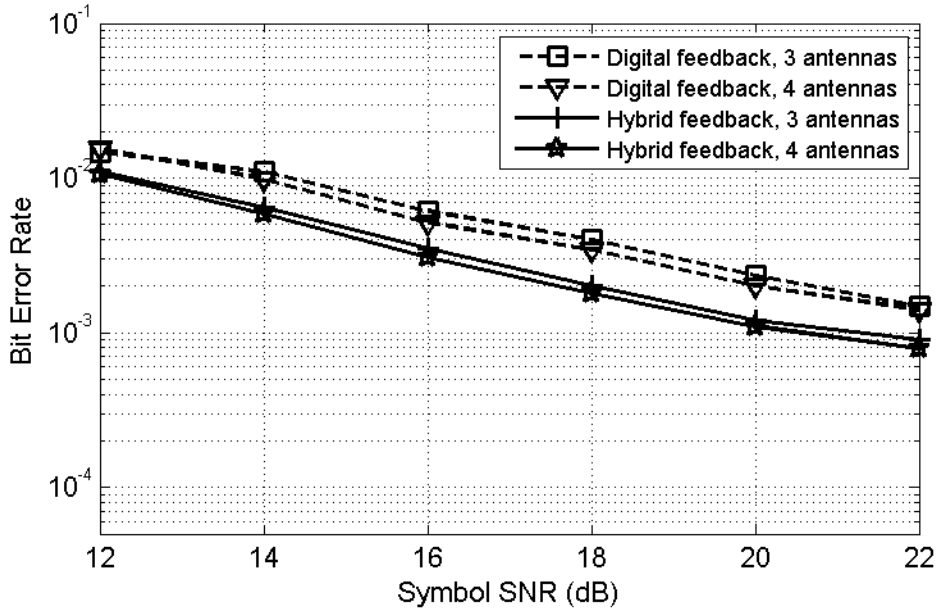

Figure 3.4-4 BER of hybrid and digital feedback in fast fading channel; $f_d T = 0.005$.

Figure 3.4-5 to Figure 3.4-7 demonstrate the closed-loop system under different operating conditions. Shown in Figure 3.4-5 and Figure 3.4-6 are the effect of different codebook size in block fading and fast fading environments. For the 3-bits IEEE 802.16e codebook, BPSK modulation is used in the feedback uplink. Thus, the feedback rate for using the 3-bits and 6-bits codebook is identical. Figure 3.4-5 shows that in block fading, the 6-bits codebook out-performs the 3-bits codebook, and hybrid feedback still out-performs digital feedback. Interestingly, 3-bits digital feedback performs better than 3-bits hybrid feedback in Figure 3.4-6. This is due to the performance of hybrid feedback is heavily dependent on the use of linear prediction. When the quantization noise is high, it becomes difficult for the predictor to output accurate result.

Finally, Figure 3.4-7 shows the effect of feedback delay on BER performance. The minimum delay is equivalent to the number of feedback symbols, which are $D = 3$ for digital feedback and $D = 4$ for hybrid feedback. It is expected that hybrid feedback have a much higher tolerance to feedback delay, since delay has been taken into account in the linear predictor design. Figure 3.4-7 verifies that using hybrid feedback lessen the performance degradation cause by feedback delay.

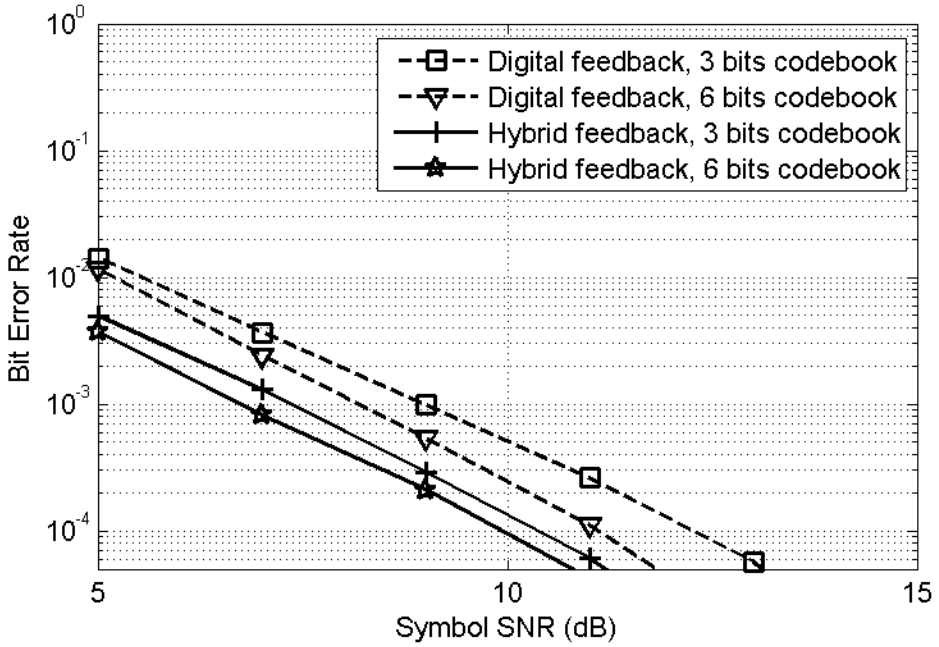

Figure 3.4-5 BER of hybrid and digital feedback in block fading channel; Different codebook size; 4 antennas

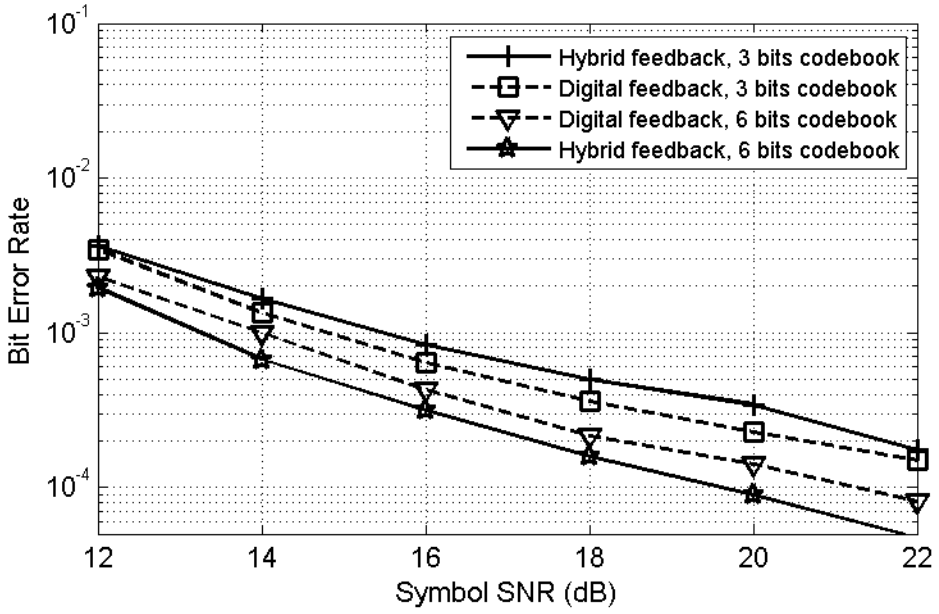

Figure 3.4-6 BER of hybrid and digital feedback in fast fading channel; Different codebook size; 4 antennas

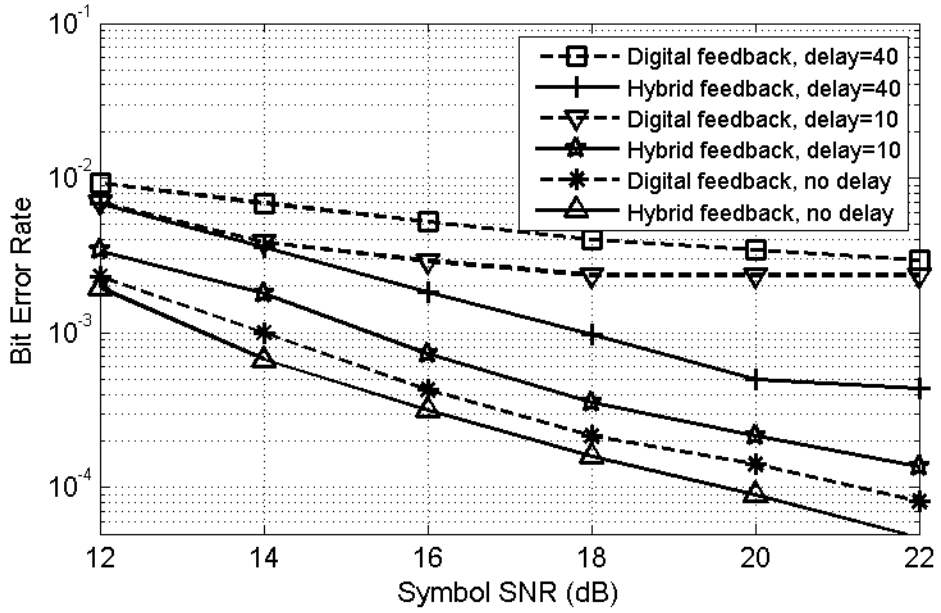

Figure 3.4-7 BER of hybrid and digital feedback in fast fading channel; Different feedback delay; 4 antennas; 6 bits codebook.

3.5 Chapter Summary

In this chapter, we consider the effectiveness of a hybrid feedback scheme in a MISO beamforming system with non-ideal CSI feedback. The hybrid feedback method effectively adapts the codebook to the channel estimate at the cost of one additional analog symbol per feedback cycle. Both block fading and time-selective fading channels are considered in our simulation. Since hybrid feedback is able to utilize linear prediction to combat fast fading, in most scenarios it is shown to offer improved BER performance when compared to the traditional digital-only feedback scheme.

CHAPTER 4 PURE ANALOG FEEDBACK IN MULTI-USER MIMO SYSTEMS

In Chapter 3, we discuss the use of codebook-based hybrid feedback and digital feedback for a MISO system. In principle, hybrid feedback utilizes the codebook as a vector quantizer to digitize the downlink channel. With the analog side information on amplitude and phase, it is able to achieve better BER performance in comparison to the alternate digital-only feedback scheme.

Nevertheless, quantizing the channel gain reduce the fidelity of the CSI. We revisit the use of pure analog CSI as the means for direct, non-quantized channel feedback. In [22], it has been shown that for a single user MISO system, analog feedback is superior to digital feedback with comparable overhead. In this chapter, we extend the investigation in [22] and examine the effectiveness of analog feedback in a multi-user MIMO system with MMSE precoding operating in time-varying fading channels. To our best knowledge, this combination of analog feedback and time-selective fading in a multi-user MIMO setting has not been considered in the literature.

This chapter starts with a brief review of analog CSI feedback and its performance improvement over digitized CSI feedback. MMSE MIMO precoding with user selection is detailed in Section 4.2. For comparison purpose, unitary precoding, an alternative codebook based precoder design scheme is the subject

in Section 4.3. Simulation result is shown in Section 4.4 and Section 4.5 is the chapter summary.

4.1 Analog Feedback Review

With analog feedback, the mobile stations simply transmit a power-scaled version of the estimated downlink channel gain directly as the feedback CSI as it is. In every feedback cycle, a mobile obtains its channel estimates $\hat{g}_l = g_l + n_l$, $l = 1, 2, ..., L$ using pilot symbol estimation described in Section 2.4. As mentioned earlier, we advocate the use of analog feedback to transmit the estimates $\hat{g}_l$ from every mobile user back to the base station. Specifically, the L uplink CSI symbols from any mobile assume the form $u[l] = \hat{g}_l / \sqrt{\sigma_g{}^2 + \sigma_n{}^2}$, $l = 1, 2, ..., L$, where $\sigma_g{}^2$ is the variance of the channel gain g and $\sigma_n{}^2$ is the variance of AWGN noise n. The normalization by $\sqrt{\sigma_g{}^2 + \sigma_n{}^2}$ ensures that $u[l]$ has an average energy of unity.

For illustrative purpose, we introduce a CSI feedback scheme that makes use of scalar quantizers derived via the LBG algorithm [25]. The in-phase (I) and quadrature (Q) components of $\hat{g}_l = g_l + n_l, l = 1, 2, ..., L$ are quantized separately and the two quantized signals are then mapped into a unit-energy QAM symbol for transmission.

To digitize each $\hat{g}_l$, its I-Q components are encoded into a pair of $\chi/2$ bits codewords using separate scalar quantizers. The quantizer has $2^{\chi/2}$ levels and is designed using Lloyd algorithm [26] to minimize the mean square error distortion between $\hat{g}_l$ and its quantized counterpart $\ddot{g}_l$

$$\begin{aligned}\varepsilon &= E\left[\left|\mathrm{Re}\{\hat{g}_l\}-\mathrm{Re}\{\ddot{g}_l\}\right|^2\right] \\ &= E\left[\left|\mathrm{Im}\{\hat{g}_l\}-\mathrm{Im}\{\ddot{g}_l\}\right|^2\right],\ l=1,2,...,L\end{aligned}. \qquad \textbf{(4.1.1)}$$

Altogether, $\hat{g}_l$ is represented by an χ bits codeword. The codeword is then Gray mapped into a square QAM CSI symbol $u_{qam}[l]$ with constellation size 2^{χ}.

We also make comparison with a vector quantized CSI feedback approach. As shown in Chapter 3, hybrid feedback quantization offers better performance than the traditional codebook feedback quantization. Therefore, hybrid feedback will be use as the representative for vector quantization. As a reminder, the hybrid feedback representation of the downlink channel gain is a combination of a quantized vector component $\mathbf{v}$ (3.2.2) and an analog component a (3.2.3). The recovered channel gain vector is define as $\tilde{\mathbf{g}}^T = a\mathbf{v}$,

where $\mathbf{v} = \arg\min_{i=1,2,...,2^B}\left\|\frac{\hat{\mathbf{g}}^T}{a}-\mathbf{v}_i\right\|^2 = \arg\min_{i=1,2,...,2^B}\left\{\mathrm{Re}\left[\hat{\mathbf{g}}^T\mathbf{v}_i^H e^{-j\theta_1}\right]\right\}$.

While analog CSI feedback is not as popular as codebook-base limited feedback, it offers several strategic advantages. Analog feedback does not

involve quantization of the downlink channel gain estimates, therefore it avoids the unrecoverable distortion from quantization. Additionally, analog feedback is simpler than codebook-based feedback from computational standpoint. This is because using a B bits codebook requires an exhaustive search through all 2^B codewords, whereas analog CSI symbols require no additional processing. The latter option is more attractive for mobile station with limited processing power and constrained CSI feedback delay requirement.

We will compare the accuracy of the feedback CSI over a non-ideal uplink channel to emphasize the difference between analog feedback, QAM feedback (scalar quantization), and hybrid feedback (vector quantization). Feedback accuracy is quantified using feedback CSI SNR defined as

$$CSI\ SNR = \frac{\frac{1}{2}E\left[\left|g_l\right|^2\right]}{\frac{1}{2}E\left[\frac{1}{L}\sum_{l=1}^{L}\left|\tilde{g}_l - g_l\right|^2\right]} = \frac{\sigma_g^2}{\frac{1}{2L}E\left[\sum_{l=1}^{L}\left|\tilde{g}_l - g_l\right|^2\right]} \quad \textbf{(4.1.2)}$$

where $\tilde{g}_l$ is the downlink gain estimate recovered by the base station and g_l is the actual downlink gain. The superiority of analog feedback accuracy can be verified via computer simulation. Consider the case which the base station is equipped with 4 antennas, $L = 4$; A 4 levels quantizer is used for scalar quantization with the result mapped to 16-QAM symbols; hybrid feedback

scheme use a 6 bits codebook with the index modulated into 3 QPSK symbol, resulting a total of 4 CSI symbols (3 QPSK + 1 analog). Overall, the number of feedback symbols and thus the feedback throughput for the three feedback schemes is identical. Curves in Figure 4.1-1 shows analog feedback CSI SNR improves with increasing symbol SNR. The 16-QAM feedback CSI SNR eventually level off at high SNR as the result of unrecoverable quantization error. In comparison, hybrid feedback has noticeably worse performance. The 16-QAM feedback uses 4 bits/antennas and therefore 16 bits are used to embed the channel gains information. In contrast, without the analog side information, the channel gain in hybrid feedback is encapsulated into 6 bits, which leads to higher quantization noise even though vector quantization is being used. Besides, in16-QAM feedback, the channel gain for each downlink antenna is independent, and therefore the CSI carried by each 16-QAM symbols can be individually decoded. When a CSI decoding error occurs, the erroneous channel gain is localized to a single antenna. Furthermore, the error is likely to be mitigated by the multi-antenna diversity effect in the downlink. In contrast, when the codebook index is off by a single bit, the entire recovered channel gains vector could be vastly different the actual gain vector, resulting in a beamforming vector that might actually further deteriorate the quality of downlink channel. One scenario which hybrid feedback may perform better than 16QAM feedback is when its underlying vector quantizer has very high resolution, e.g. 12 bits (mapped into three 16QAM

symbols, plus 1 analog symbol) . Unfortunately, such a codebook is not readily available in the literature.

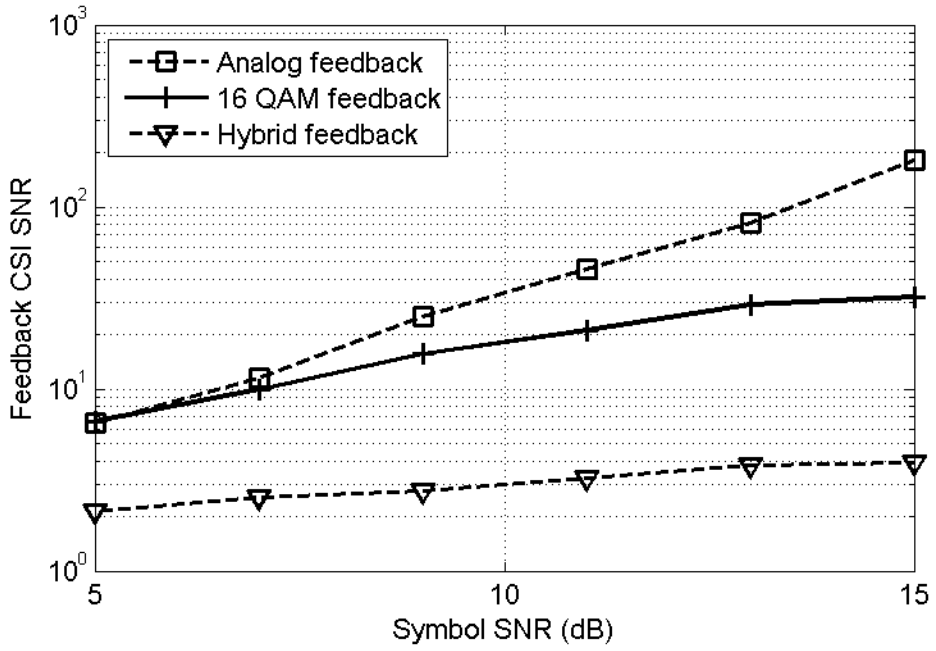

Figure 4.1-1 Feedback CSI SNR. $f_d T = 0.002$

In a fast fading multi-user MIMO environment, the requirement for feedback accuracy is even more stringent. This is due to the phenomenon of multi-user interference. Unlike singleuser system, where performance can be shown to be limited by transmission power, the performance of a multi-user system is often interference-limited. Interference cancellation through channel inversion is a main objective for the multi-user MMSE precoder design. The MMSE precoder is only effective when the channel matrix obtained through CSI feedback is sufficiently accurate. From the high irreducible distortion for the

recovered downlink channel gain shown in the CSI SNR, the low-resolution hybrid feedback scheme is not expected to operate well in a MIMO setting.

4.2 MMSE MIMO Precoding

As explained in Section 2.2.2, we consider a base station with L antennas transmitting to Z mobile users out of a pool of M users. In order to satisfy the dimensionality constraint, we require that $L \geq Z$. Each mobile user is equipped with a single antenna and consequently there are $L \times M$ downlink propagation paths between the base station and the users. For notation brevity, the fading gain in any downlink path at symbol position k is given the general notation $g[k]$, and the AWGN at any mobile receiver is given the general notation $n[k]$. When necessary, subscripts will be added to $g[k]$ and $n[k]$ to highlight the specific link/antenna. On other occasions, we drop the symbol index k for the sake of notation brevity, but it should be understood that the underlying processes actually vary with time.

Using the procedures described in the previous section, a mobile converts its channel estimates $\hat{g}_l = g_l + n_l, l = 1, 2, ..., L$ into L analog or QAM CSI symbols. Each user sends its CSI symbols to the base station using the PSAM procedure described in Section 2.3. Now, let $\hat{u}_z[l]$ denotes the CSI recovered at the base station for the $l-th$ downlink paths of the $z-th$ user, and define $\hat{\mathbf{u}}_z = \left(\hat{u}_z[1], \hat{u}_z[2], ..., \hat{u}_z[L]\right)$. Because of the need to perform user selection, the

base station will analyze all $\binom{M}{Z}$ combinations of CSI vectors in the set $\{\hat{\mathbf{u}}_1, \hat{\mathbf{u}}_2, ..., \hat{\mathbf{u}}_M\}$, and selects the "best" group of Z users. To explain the proposed user selection procedures, we use the notation

$$\hat{\mathbf{G}} = \sqrt{\sigma_g{}^2 + \sigma_n{}^2}\left(\hat{\mathbf{u}}_{i_1}^T, \hat{\mathbf{u}}_{i_2}^T, ..., \hat{\mathbf{u}}_{i_Z}^T\right)^T \quad \textbf{(4.2.1)}$$

to represent the estimated channel matrix for an arbitrary group of Z users. It should be understood that each i_z is from the set $\{1, 2, ..., M\}$ and no two i_z's are identical. Elements of this matrix are simply the base-station's estimates of the downlink channel gains between its antennas and the group of users. We emphasize that (4.2.1) is simply the channel estimate of the downlink during the pilot transmission phase of a downlink frame. Similar to the prediction technique used in Chapter 3, linear prediction can be used to estimate the actual gains affecting the data symbols.

Assume the base station has selected a group of users. Let s_z denotes the data symbol intended for the $z-th$ member of this selected group at an arbitrary symbol position in the current frame, where each s_z is drawn from a unit-energy signal constellation. The Z data symbols $\mathbf{s} = \left(s_1, ..., s_Z\right)^T$ are transmitted over the L antennas using an $L \times Z$ MMSE precoder $\mathbf{W}$. The precoded signal is

$$\mathbf{x} = \mathbf{W}\mathbf{s}/\sqrt{\beta}\,. \tag{4.2.2}$$

In addition, the composite received signal of the Z selected users is

$$\mathbf{r} = \mathbf{G}\mathbf{x} + \mathbf{n}\,, \tag{4.2.3}$$

where $\beta = \|\mathbf{W}\mathbf{s}\|^2$ is a power normalization factor, $\mathbf{G}$ is an $Z \times L$ channel matrix containing the complex gains in the $Z \times L$ links between the base station and the selected mobiles, and $\mathbf{n}$ an $Z \times 1$ AWGN vector. Note that individual components of $\mathbf{G}$ and $\mathbf{Z}$ assume the general statistics of $g[k]$ and $n[k]$ described in Section 2.2.1. Furthermore, the matrix $\hat{\mathbf{G}}$ in (4.2.1) is a dated and noisy version of $\mathbf{G}$.

Now, substituting (4.2.2) into (4.2.3) and multiplying both sides by $\sqrt{\beta}$ allows us to obtain

$$\hat{\mathbf{s}} = \sqrt{\beta}\mathbf{r} = \mathbf{G}\mathbf{W}\mathbf{s} + \sqrt{\beta}\mathbf{n}\,, \tag{4.2.4}$$

As demonstrated in [13], if $\mathbf{G}$ is known perfectly at the base station, then we can choose the precoder $\mathbf{W}$ in such a way that the mean square value of

$$e = \mathbf{s} - \hat{\mathbf{s}} = \mathbf{s} - (\mathbf{G}\mathbf{W}\mathbf{s} + \sqrt{\beta}\mathbf{n})\,. \tag{4.2.5}$$

is minimized. This leads to the so-call MMSE precoder. Let

$$
\begin{aligned}
\varepsilon &= E\left\|e\right\|^2 \\
&= E\left[tr(ee^H) \right] \\
&= tr(((\mathbf{I}-\mathbf{GW})(\mathbf{I}-\mathbf{GW})^H + tr(\mathbf{WW}^H)\sigma_n^2\mathbf{I})/Z \\
&= tr([\mathbf{I}-\mathbf{GW})(\mathbf{I}-\mathbf{GW})^H]/Z) + tr(\mathbf{WW}^H)\sigma_n^2 \\
&= tr(\mathbf{GWW}^H\mathbf{G}^H - \mathbf{GW} - \mathbf{W}^H\mathbf{G}^H + \mathbf{I} + Z\sigma_n^2\mathbf{W}^H\mathbf{W})/Z
\end{aligned}
\quad . \qquad \textbf{(4.2.6)}
$$

By setting $\frac{\partial \varepsilon(\mathbf{W})}{\partial \mathbf{W}} = \mathbf{W}^H\mathbf{G}^H\mathbf{G} - \mathbf{G} + Z\sigma_n^2\mathbf{W}^H\mathbf{W} = 0$, the optimum precoding matrix can be obtained as

$$
\mathbf{W} = \mathbf{G}^H(\mathbf{GG}^H + K\sigma_n{}^2\mathbf{I})^{-1}. \qquad \textbf{(4.2.7)}
$$

Equations (4.2.6) and (4.2.7) forms the basis of user selection, as we shall describe next. According to (4.2.7), the "best" group of users is the group whose $\mathbf{G}$ matrix minimizes the MSE. As long as M is not unreasonably large, this can be done through an exhaustive search over all $\binom{M}{Z}$ possibilities. However, two minor modifications to (4.2.6) and (4.2.7) are required before executing this search. Firstly, we need to replace $\mathbf{G}$ in these equations by its estimate $\tilde{\mathbf{G}}$, since in practice, $\mathbf{G}$ is not known precisely. Secondly, the channel is time-varying, consequently $\mathbf{G}$, and hence $\mathbf{W}$ and ε, are also time-varying. To deal with these issues, we consider a user selection strategy that calculates an estimated MSE base on the predicted channel response.

In our user selection strategy, the base-station uses the feedback CSI $\hat{\mathbf{G}}$ in (4.2.1) received for the current downlink frame, as well as those received for

the J previous frames, to estimate/predict the channel matrix $\mathbf{G}$ at every symbol positions in the current frame. The estimate $\tilde{\mathbf{G}}$ is then substituted into (4.2.6) and (4.2.7) to obtain the MSE at a particular data symbol position. Let $\tilde{\mathbf{G}}[k]$ be the predicted version of $\mathbf{G}[k]$ for the $k-th$ symbol in the current frame, then the user selection process computes for every user group the sum MMSE across the entire frame:

$$\varepsilon_{frame} = \sum_{k=1}^{F} \mathrm{tr}((\mathbf{I} - \tilde{\mathbf{G}}[k]\mathbf{W}[k])(\mathbf{I} - \tilde{\mathbf{G}}[k]\mathbf{W}[k])^{H}) / Z + \mathrm{tr}(\mathbf{W}[k]\mathbf{W}^{H}[k])\sigma_n{}^2, \qquad \textbf{(4.2.8)}$$

where $\mathbf{W}[k]$ is equivalent to $\mathbf{W}$ in (4.2.6) but with $\mathbf{G}$ replaced by $\tilde{\mathbf{G}}[k]$. The group with the smallest ε_{frame} is selected. The process is repeated every frame-cycle. It should be emphasized that while the selected group of users is only updated once per frame, the precoder itself changes at every data symbol position. This is because by substituting $\tilde{\mathbf{G}}$ for $\mathbf{G}$ in (4.2.7), the precoder is able to track the time-variation in the fading channel.

4.3 Unitary Precoding

We will compare the BER of the proposed multi-user MMSE precoders with analog feedback against their counterparts based on QAM feedback. In addition, we will also make comparisons against codebook-based unitary precoders [15]. In unitary precoding, each user finds its optimum precoder out of a finite set of precoders. The selection is based on channel quality indicator,

which is usually chosen to be the SINR calculated at the mobile. We assume a B bits unitary matrix codebook with entries $\{\mathbf{V}_1,...,\mathbf{V}_{2^B}\}$, where each $\mathbf{V}_q = \{\mathbf{v}_{1,q},...,\mathbf{v}_{P,q}\}$, $1 \le q \le 2^B$, is a unitary matrix with P orthogonal columns. Each column vector can be used as a precoding vector corresponds to one of the mobile's downlink channel. The unitary codebook contains a total of $P \times 2^B$ unit vector candidates for precoding vector selection.

Upon obtaining the channel estimate $\hat{\mathbf{g}} = (\hat{g}_1, \hat{g}_2, ..., \hat{g}_L)$ from the downlink pilots, each mobile compute its channel quality indicators, denoted as $SINR_{p,q}$,

$$SINR_{p,q} = \frac{|\hat{\mathbf{g}}^{\dagger}\mathbf{v}_{p,q}|^2}{L\sigma_n{}^2 + \sum_{o \neq p} |\hat{\mathbf{g}}^{\dagger}\mathbf{v}_{o,q}|^2}, \quad 1 \le p \le P, 1 \le q \le 2^B. \qquad \textbf{(4.3.1)}$$

When a user computes $SINR_{p,q}$, it assumes it has been assigned the $p-th$ column vector in the $q-th$ unitary matrix, whereas the remaining $P-1$ column vectors are assigned to the other users. Ideally, $\hat{\mathbf{g}}$ should lie in the null space form by the $P-1$ non-chosen column vectors, and therefore the user would experience zero multi-user interference. In practice, since a codebook has finite resolution, there will always be some interference power as the result of quantization distortion.

Each user can send back a total of $P \times 2^B$ $SINR_{p,q}$ CSI symbols, $p \in \{1, 2, ..., P\}$ and $q \in \{1, 2, ..., 2^B\}$. Compare to only L CSI symbols required for

MMSE precoding with analog/QAM feedback, unitary precoding generates a much higher volume of feedback traffics in the uplink. Consider that we assume a noisy uplink structure with non-zero feedback delay, full $SINR$ feedback is only feasible with an extremely high-rate feedback link. Alternatively, we could consider limited feedback scheme that greatly reduce feedback rate by omitting a portion of $SINR$ values.

A medium-rate feedback strategy is to only feedback the index of the precoder that offers the maximum sum rate, i.e.,

$$q = \arg\max_{q\in\{1,2,...,2^B\}} \sum_{p=1}^{P} \log(1+SINR_{p,q}), \quad \textbf{(4.3.2)}$$

and the corresponding P $SINR_{p,q}$ values, $p \in \{1,2,...,P\}$.

A low-rate feedback strategy is to only feedback the optimum precoder index and the optimum precoding vector index, i.e.,

$$(p,q) = \arg\max_{p\in\{1,2,...,P\}\times q\in\{1,2,...,2^B\}} \log(1+SINR_{p,q}) \quad \textbf{(4.3.3)}$$

In this scenario, no $SINR$ needs to be feedback at all. Only the optimum indices P and Q are required. When using medium or low-rate feedback strategy, the base station sets the missing $SINR$ values to zero.

Let the set of $SINR$ values from the $z-th$ user be denoted by $SINR^z$. The objective of the selection is to find the optimal precoder for a set of compatible

users. Each precoding vector in this precoder should maximizes the receive SNR for one user, while simultaneously generates minimum amount of interference power for the other $Z-1$ users. With M total users, the base station has to process $\begin{pmatrix} M \times P \times 2^B \\ Z \end{pmatrix}$ $SINR$ combinations to find the optimum user set. Clearly, finding the optimal user set through exhaustive search is computationally expensive and difficult to accomplish in a timely manner. Instead, the Per User Unitary Rate Control (PU2RC) algorithm in [15] can be used to greatly simplify the user selection process. The algorithm is further explained in Appendix 2.

We note that if medium feedback or low-rate feedback are deployed, then it is possible for the algorithm to schedule less than Z users due to the missing $SINR$ values. Therefore, downlink throughput suffers as the result of uplink feedback rate reduction. Even worse, the base station cannot extract the actual downlink channel gain from the $SINR$ CSI and therefore, the base station will not be able to make use of linear prediction. As a result, unitary precoding is expected to be ineffective against time-selective fading.

4.4 Simulation Results and Discussion

Many simulation parameters used in the evaluation of multi-user MIMO system are similar to those used in the Section 3.4 simulation. The system consist of 4 transmit antennas, with 2 active users chosen from a pool of 10 users. BPSK modulation (± 1 symbols) with differential encoding (DBPSK) and

differential detection are used in the downlink to transport the data. Unless otherwise stated, each downlink frame consists of $F = 80$ data symbols and 4 pilot symbols; there is no feedback delay. For beamforming and user selection purposes, $J = 10$ order predictors are used at the base-station to predict the down link gains from the received CSI. In order to evaluate the performance of analog feedback, we considered two benchmark schemes: unitary precoding with no feedback error (Section 4.3) and MMSE precoding with QAM feedback. The simulation parameters are summarized in Table B.

Table B Simulation parameters.

Channel Type	Normalized Doppler frequency $f_d T$	Channel coherence time $1/f_d$	Channel estimation rate (approx.) $1/T_{Fr}$, $T_{Fr} = NT$	Frame size N	Number of antennas L
Block Fading	N/A			84	4
Fast fading	0.001	$1000T$	$12 f_d$		
	0.002	$500T$	$6 f_d$	84	
			$12 f_d$	44	
	0.005	$200T$	$2.5 f_d$	84	
			$5 f_d$	44	

The following naming conventions are adopted for the BER curves: (a) curves labeled **2/2** corresponds to no user selection. i.e., the total number of users in the system is 2 and they are always scheduled for transmission. (b) curves labeled **2/10** implies user selection at work: 2 active users from a pool of

10 users, (c) curves labeled **no feedback error** implies an error-free uplink, $\tilde{\mathbf{G}}$ in (4.2.8) equals the feedback CSI symbols (or, in the case of unitary precoding, the SINRs in (9) are correctly received). Note that the base station still will not be able to obtain the actual downlink gain, since there is estimation error during the pilot phase. For unitary precoding, we consider the case of full SINR feedback with no feedback error, so that the PU2RC selection algorithm will always be able to schedule 2 users for transmission. By fixing data throughput, we ensure that the BER comparisons are fair. Hybrid feedback, QAM feedback, and unitary precoding are collectively classified as digital feedback.

We start off by examining the impact of channel time-variation on system BER performance. Figure 4.4-1 to Figure 4.4-4 show the cases for channels with block fading ($f_d T = 0$), low Doppler frequency ($f_d T = 0.001$), medium Doppler frequency ($f_d T = 0.002$), and high Doppler frequency ($f_d T = 0.005$). The simulations confirm that due to low CSI SNR (see Section 4.1), hybrid feedback does not perform well in a multi-user MIMO environment. In all four cases, the analog feedback and QAM feedback curves show similar receive diversity order. The results for analog feedback are better than QAM feedback since analog feedback completely bypasses the quantization process and is thus able to avoid any unrecoverable quantization error.

In Figure 4.4-1, although MMSE precoding outperforms unitary precoding with the absence of feedback error, unitary precoding remains competitive in a

block fading environment. As fade rate increases from Figure 4.4-2 to Figure 4.4-4, the unitary precoding curves eventually reach an error floor, suggesting that the system becomes interference-limited. As expected, the performance of unitary precoding is limited by its inability to track the time-varying channel through the feedback CSI. In order to benefit from diversity gain, it requires significantly higher channel estimation rate to update the precoder and user selection decisions. We also have to keep in mind that the implemented unitary precoding assumes no feedback error and therefore, it suffers additional setback when operating in an environment with non-ideal, delay-constrained feedback uplink.

In Figure 4.4-4, none of the precoders works well in fading channels with high normalized Doppler frequency. A simple solution to deal with the high fade rate is to increase the channel estimation rate by reducing the frame size. This result is shown in Figure 4.4-5 and Figure 4.4-6. By halving the frame size, channel estimation is effectively doubled. However, efficiency of data throughput suffers since the number of pilot symbols remains unchanged. Figure 4.4-5 and Figure 4.4-6 further demonstrate that in comparison to unitary precoding, MMSE precoding have higher tolerance against fast fading.

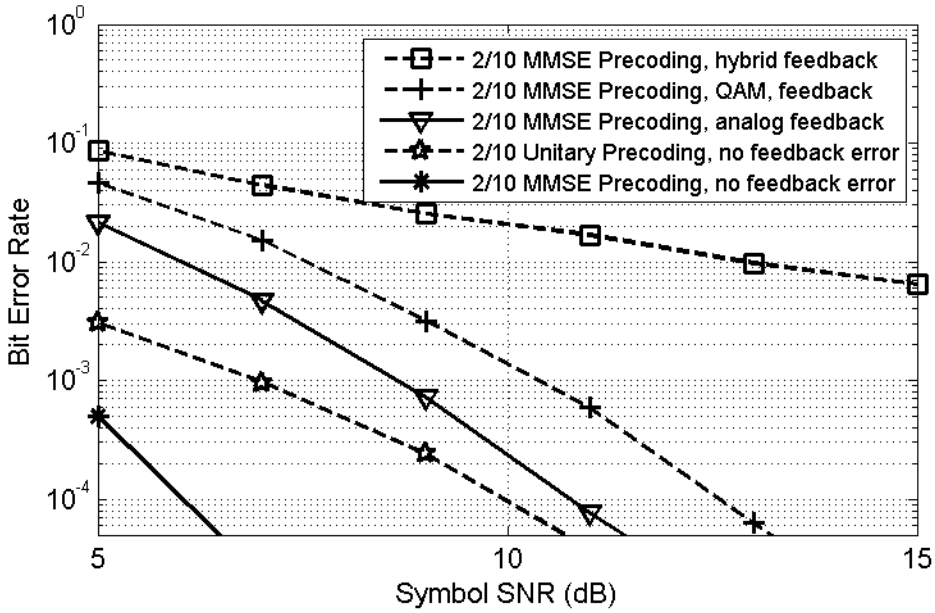

Figure 4.4-1 BER of analog and digital feedback in block fading channel; $F = 80$

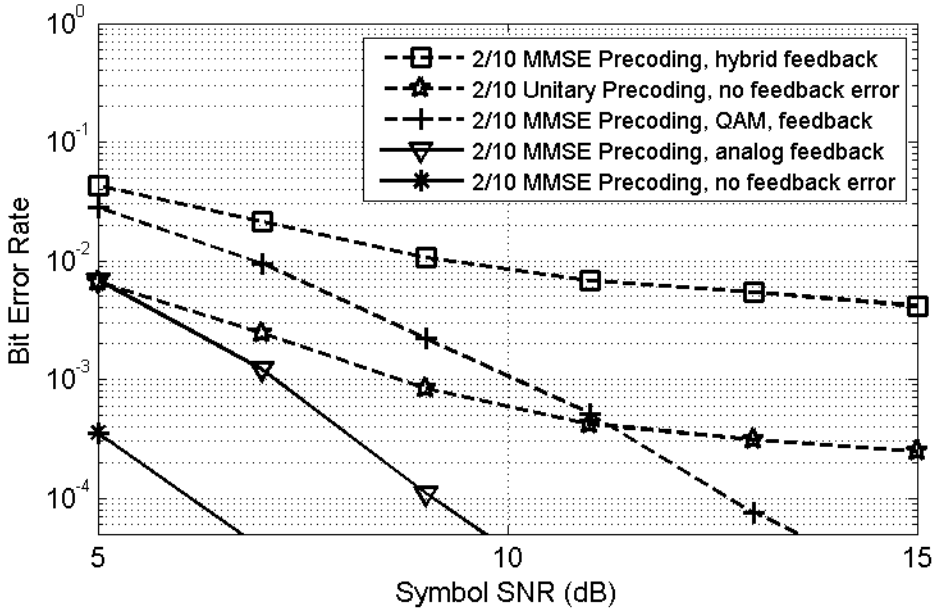

Figure 4.4-2 BER of analog and digital feedback in fast fading channel; $f_d T = 0.001$**;** $F = 80$

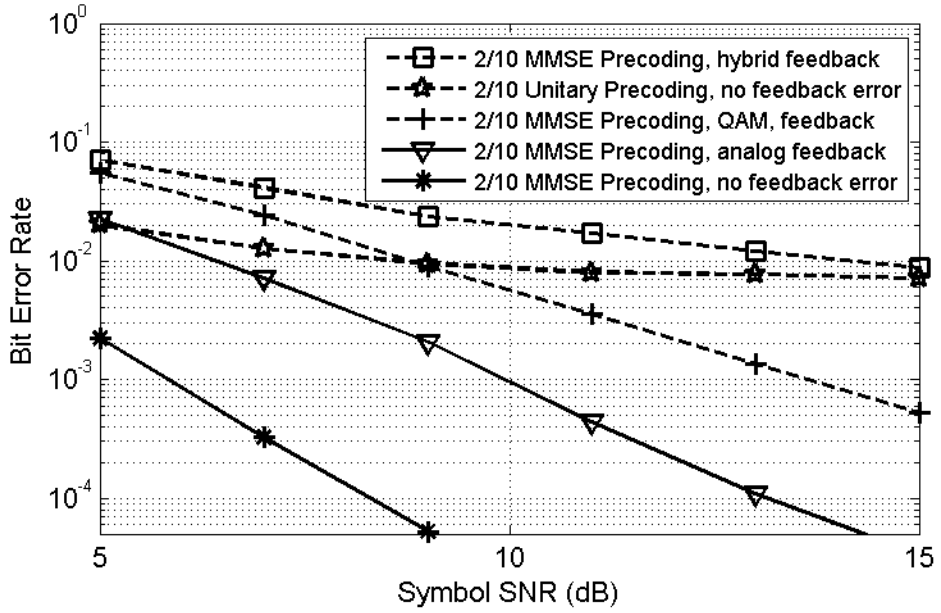

Figure 4.4-3 BER of analog and digital feedback in fast fading channel; $f_d T = 0.002$ **;** $F = 80$

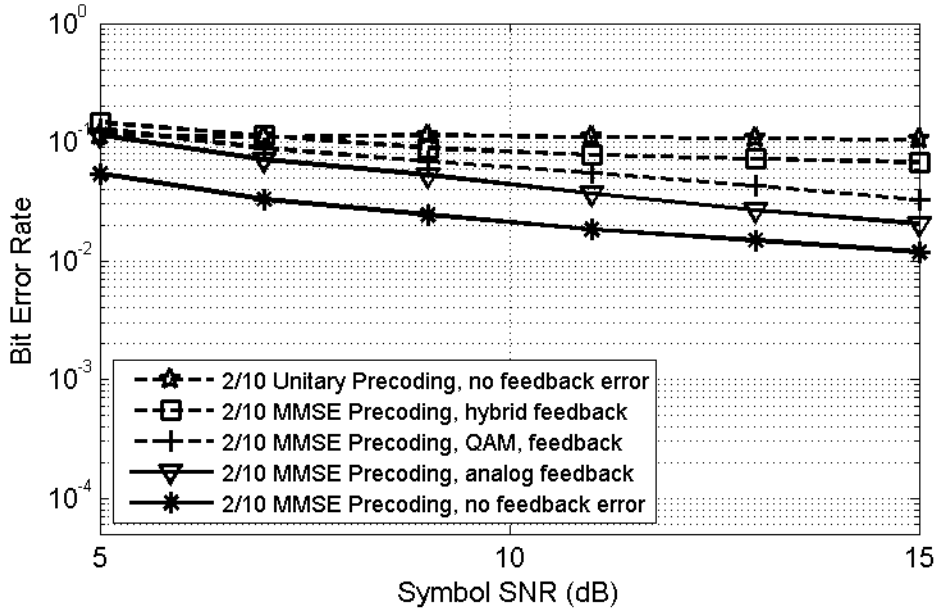

Figure 4.4-4 BER of analog and digital feedback in fast fading channel; $f_d T = 0.005$ **;** $F = 80$

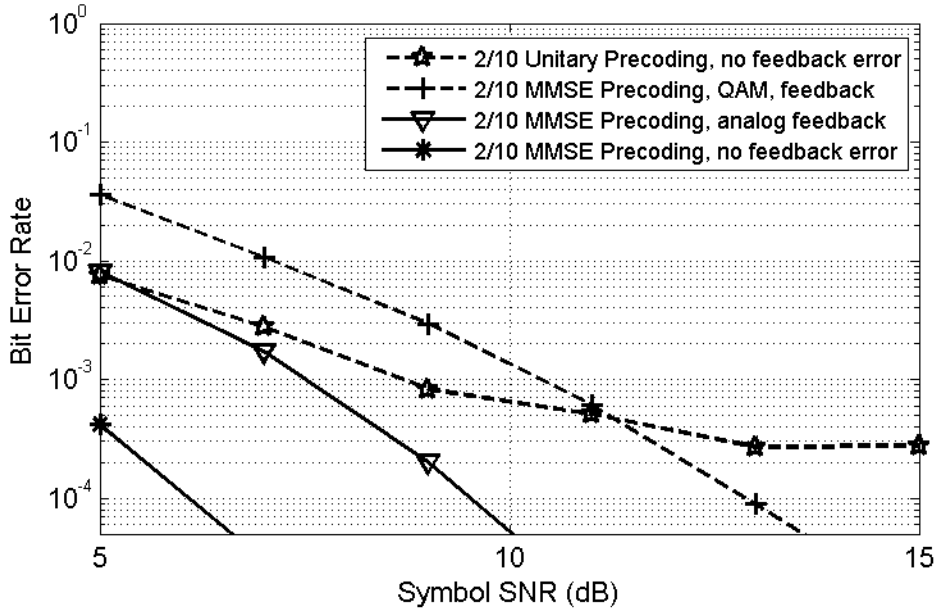

Figure 4.4-5 BER of analog and digital feedback in fast fading channel; $f_d T = 0.002$ **;** $F = 40$

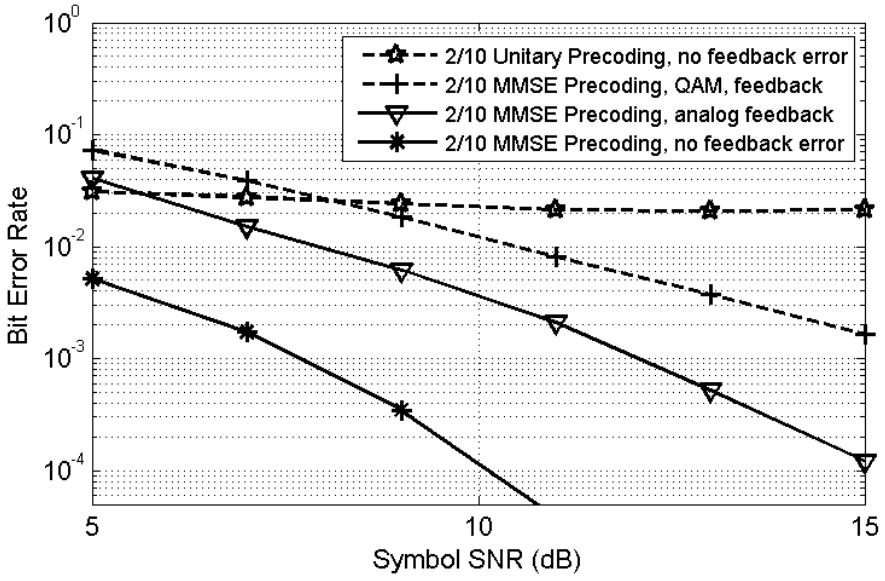

Figure 4.4-6 BER of analog and digital feedback in fast fading channel; $f_d T = 0.005$ **;** $F = 40$

To demonstrate the multi-user effect of the proposed multi-user MIMO system, we first show the effect of reducing the active user pool size from 10 in previous figures to 2 in Figure 4.4-7 and Fig. 4.4-8. Furthermore, we show in to Figure 4.4-9 the downlink BER curves for user pool of various sizes. The general conclusion is that unitary precoding has poor performance without the multi-user effect, since it is unlikely for the given users to have nearly orthogonal channels. In contrast, even without the multi-user effect, MMSE precoding demonstrates resilience against fast fading. In Figure 4.4-9, signal power is fixed to 10dB and system performance is measured as a function of user pool size. All curves show diminishing return for improvement in BER as the user pool increases. Since a large user pool is not necessary, the use of brute force method in MMSE user selection algorithm will not cause too much concern.

Finally, we show in Figure 4.4-10 the effect of feedback delay on system performance, where a delay of 4 symbols is the minimal delay that can be achieved in practice for a MMSE precoding system with 4 antennas. It is observed that as long as the delay is shorter than 10 symbols, its impact on the BER of the proposed MMSE precoders is rather minimal (less than 1dB loss at BER of 10^{-3}). A delay of 40 symbols, on the other hand, incurs a 3 dB loss in power efficiency at a BER of 10^{-3}. The diversity gain however, is not affected.

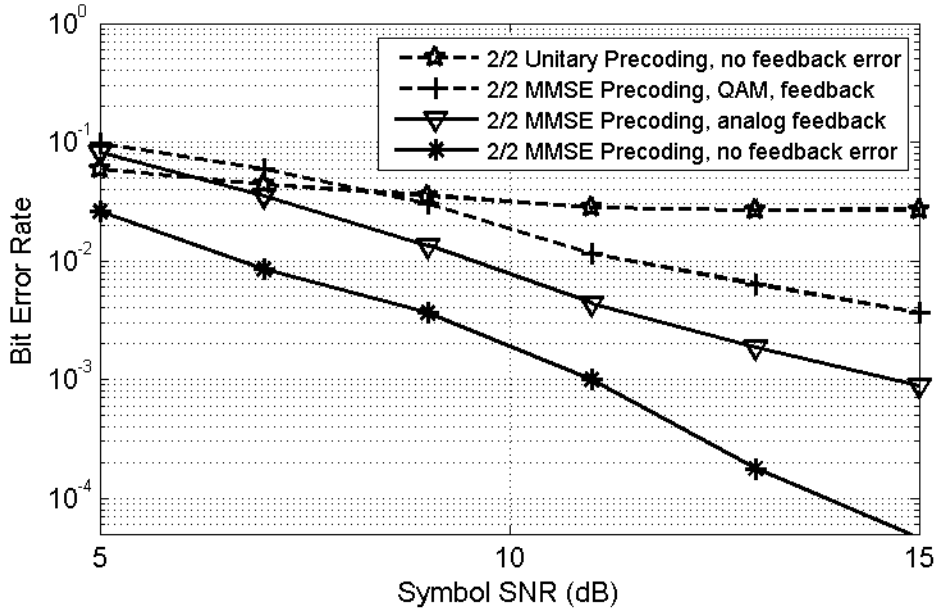

Figure 4.4-7 BER of analog and digital feedback in block fading channel; $F = 80$

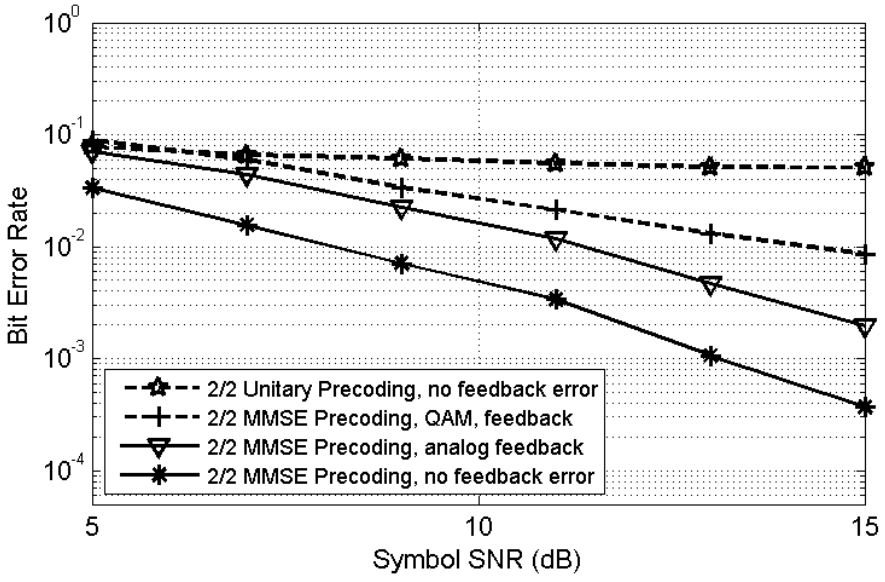

Figure 4.4-8 BER of analog and digital feedback in fast fading channel; $f_d T = 0.002$ $F = 80$

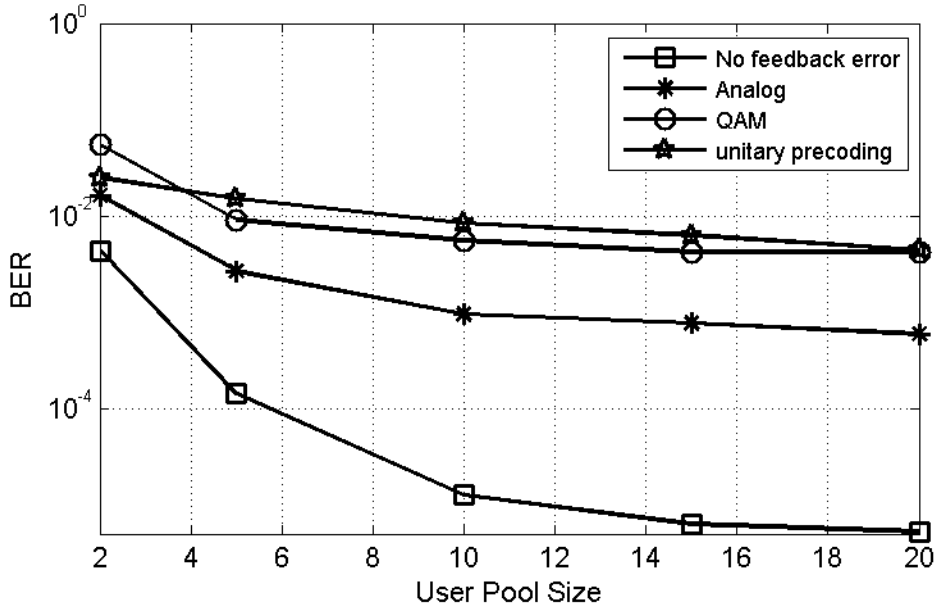

Figure 4.4-9 Multi-user effect, 2 active users; $f_d T = 0.002$ **;** $F = 80$ **;** $SNR = 10dB$

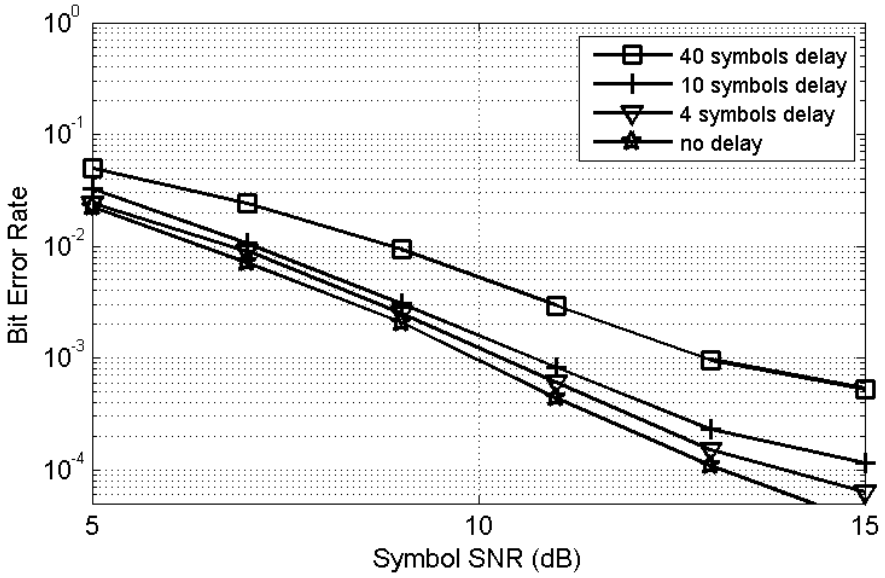

Figure 4.4-10 Feedback delay in MMSE precoding system with analog feedback; $f_d T = 0.002$ **;** $F = 80$ **;** $2/10$ *users*

4.5 Summary

In this chapter, we consider the effectiveness of a MMSE precoding technique in a multi-user MIMO environment with time-selective fading channel and non-ideal feedback. Analog CSI feedback is found to have superior BER performance over quantized CSI feedback, since it avoids the unrecoverable distortion due to digitization. By using previously received CSI symbols and linear predictor filter to extrapolate downlink channel gain at the data symbol position, MMSE precoding is able to mitigate the detrimental effects of time-selective fading. In contrast, while unitary precoding with multi-user diversity works well in a block fading environment, the performance cannot be carry over to a time-selective setting.

CHAPTER 5 CONCLUSION

In this thesis, we study two topics related to uplink CSI feedback format. For a singleuser MISO system, we present a hybrid feedback scheme that improves upon the digital feedback scheme. Codebook-base vector quantization introduces quantization distortion into the downlink channel gain estimate. We reduce this distortion by using an additional analog symbol to encapsulate channel magnitude and phase information. This feedback strategy allows the use of downlink channel linear prediction to combat time-variation in a fast fading channel. The benefit of the proposed feedback scheme is verified via computer simulation. While hybrid feedback has slightly higher uplink bandwidth, it yields superior downlink BER performance compare to digital feedback system.

For a multi-user MIMO operating environment, we examine the effectiveness of analog CSI feedback in conjunction with MMSE precoding. Since MMSE precoding is only effective when the effective channel matrix is non-singular, we incorporate multi-user selection in our design to exploit multi-user diversity gain. Since the MIMO system is expected to operate in a fast fading environment, we utilize predicted channel response in the MMSE computation. Simulation verifies that analog CSI feedback outperforms both scalar quantized CSI feedback and vector quantized CSI feedback. We also make comparison to codebook-base unitary precoding strategy that feedback SINR values. It is

shown that due to its inability to track time-variation in the fading channel, the BER performance of unitary precoding quickly deteriorates as the channel normalized Doppler frequency increases.

Suggestions for Future Research

Possible research extensions to this thesis include investigating the performance of hybrid feedback and analog feedback in other operating environments, as well as enhancing the MMSE user selection strategy.

To simplify design, our proposed system consist of mobiles equipped with a single receive antenna. An extension might involve investigating the performance of the hybrid feedback and analog feedback systems for mobiles with multiple receive antennas. In a multi-user multiple receive antennas MIMO operate environment, the current MMSE precoding strategy can still function if each user antenna is treated as a separate user. In this case, each user's receive antennas are uncoordinated. [17] has shown that receiver coordination for zero-forcing beamforming using receive combining technique is beneficial to system performance. By adding receive antenna coordination to MMSE precoding, we can generalize the MIMO structure.

The multi-user selection algorithm used in our MIMO system employs a brute-force search method to find the optimal set of users. In Section 4.4, we have shown that MMSE precoding with analog feedback does not require a large

user pool size to extract reasonable gain from multi-user diversity. Nevertheless, from a complexity perspective, the brute-force method is less attractive compared to the PU2RC algorithm used in unitary precoding. An extension to MMSE user selection algorithm might involve finding a near-optimal selection algorithm whose computation complexity grows linearly as a function of user pool size.

APPENDIX 1: GRASSMANNIAN CODEBOOK

The use of Grassmannian codebook design for MIMO system is introduced in [7]. The Grassmannian design criterion exploits the relationship between the CSI quantization problem and Grassmannian line packing [27]. In [7], it has been shown that in terms of average received signal to noise ratio, Grassmannian line packing provides the optimal codebook design under spatial uncorrelated MIMO channel.

The codebook aims to provide a set of matrices that maximize the minimum subspace distance between any pair of lines. Suppose we represent a packing of $L \times 2^B$ matrix $\mathbf{V} = [\mathbf{v}_1 \quad \mathbf{v}_2 \quad ... \quad \mathbf{v}_{2^B}]$ whose column space $\mathbf{v}_i$ is the $i-th$ line in the packing. $\mathbf{v}_i$ is a unit vector with $\mathbf{v}_i{}^H \mathbf{v}_i = 1$ and $\mathbf{v}_j{}^H \mathbf{v}_i \neq 1 (i \neq j)$. The chordal distance metric[4] $d(\mathbf{v}_1, \mathbf{v}_2)$ is defined as the angle $\theta_{1,2}$ between the two lines generated from the unit vectors $\mathbf{v}_1$ and $\mathbf{v}_2$. The chordal distance is

$$d(\mathbf{v}_1, \mathbf{v}_2) = \sin(\theta_{1,2}) = \sqrt{1 - \left| \mathbf{v}_1^H \mathbf{v}_2 \right|^2} \qquad \textbf{(A.1)}$$

The minimum distance of a packing is the sine of the smallest angle between any pair of lines, which can be written as

[4] Besides the chordal distance, other subspace distance metric such as spectral distance and Fubini-Study distance can also be used

$$\delta(X) = \min_{1 \le j < l \le 2^B} \sqrt{1 - \left| \mathbf{v}_j^H \mathbf{v}_l \right|^2} \qquad \textbf{(A.2)}$$

Finally, a Grassmannian codebook is designed by solving

$$\mathbf{V} = \arg\max_{X \in |X| = 2^B} \delta(X) \qquad \textbf{(A.3)}$$

The Grassmannian codebook used in this thesis is constructed using the codebook generation operation defined in the IEEE802.16 standard [24]. Let the notation $\mathbf{V}(L, Z, B)$ denotes the vector codebook that consists 2^B complex unit vectors of dimension L, and Z denotes the number of data streams (users). The integer B is the number of bits required for the codebook index. In Section 8.4.5.4.10.15 in the IEEE802.16 standard, Table 298p provides the generating parameters $\mathbf{u}$ and $\mathbf{s}$ for $\mathbf{V}(3,1,6)$ and $\mathbf{V}(4,1,6)$. The predefined values are reproduced in Table C.

Table C Generating parameters for $\mathbf{V}(3,1,6)$ and $\mathbf{V}(4,1,6)$

L	B	**u**	**s**
3	6	[1 26 57]	[1.2518–-j0.6409, –0.4570–*j*0.4974, 0.1177+*j*0.2360]
4	6	[1 45 22 49]	[1.3954–*j*0.0738, 0.0206+*j*0.4326, –0.1658–*j*0.5445, 0.5487–*j*0.1599]

Based on $\mathbf{u}$ and $\mathbf{s}$, the codebook can be construct using the following operations. The first codebook vector $\mathbf{V}_1$ is simply a unit vector whose entries are equally spread out on the unit circle.

$$\mathbf{v}_1 = \frac{1}{\sqrt{L}}\left[1 \quad e^{j\frac{2\pi}{L}} \quad ... \quad e^{j\frac{2\pi}{L}(L-1)}\right]^T. \tag{A.4}$$

Then, a unitary $L \times L$ matrix $\mathbf{H}(s)$, which takes $\mathbf{s}$ as a parameter is generated using

$$\mathbf{H}(s) = I - p\mathbf{v}\mathbf{v}^H \tag{A.5}$$

where $\mathbf{v} = \mathbf{s} - [1 \quad 0 \quad ... \quad 0]_{1\times L}$, $p = \frac{2}{\left\|\mathbf{v}^H\mathbf{v}\right\|}$. All the codewords $\mathbf{v}_i, i = 2,3,...,2^B$ are derived from the first codeword $\mathbf{v}_1$ based on

$$\tilde{\mathbf{v}}_i = \mathbf{H}(s)\mathbf{Q}^i(u)\mathbf{H}(s)^H \mathbf{v}_1, i = 2,3,...,2^B \tag{A.6}$$

$$\mathbf{v}_i = \tilde{\mathbf{v}}_i e^{-j\phi_1} \tag{A.7}$$

where $\mathbf{Q}^i(u)$ is a rotational matrix

$$\mathbf{Q}^i(u) = diag\left(e^{j\frac{2\pi}{2^B}u_1 \cdot i} \quad e^{j\frac{2\pi}{2^B}u_2 \cdot i} \quad ... \quad e^{j\frac{2\pi}{2^B}u_L \cdot i}\right) \tag{A.8}$$

Finally, the codewords are rounded to four decimal places. Note that due to (A.7), the first entry of every code vector is a real number. The codewords in $\mathbf{V}(3,1,6)$ are reproduced in Table D as a reference

Table D Entries for codewords in codebook $\mathbf{V}(3,1,6)$

Matrix index	Column	Matrix index	Column
000000	0.5774 -0.2887 + j0.5000 -0.2887 - j0.5000	010000	0.3169 0.4970 + j0.1434 -0.6723 + j0.4243
000001	0.5466 0.2895 – j0.5522 0.2440 + j0.5030	010001	0.7031 -0.4939 – j0.4297 0.2729 – j0.0509
000010	0.5246 -0.7973 – j0.0214 -0.2517 – j0.1590	010010	0.3649 0.1983 + j0.7795 -0.3404 + j0.3324
000011	0.5973 0.7734 + j0.0785 0.1208 + j0.1559	010011	0.6658 0.2561 – j0.6902 -0.0958 – j0.0746
000100	0.4462 -0.3483 – j0.6123 -0.5457 + j0.0829	010100	0.3942 -0.3862 + j0.6614 0.0940 + j0.4992
000101	0.6662 0.2182 + j0.5942 0.3876 – j0.0721	010101	0.6825 0.5632 + j0.0490 -0.1901 – j0.4225
000110	0.4120 0.3538 – j0.2134 -0.8046 – j0.1101	010110	0.3873 -0.4531 – j0.0567 0.2298 + j0.7672
000111	0.6840 -0.4292 + j0.1401 0.5698 + j0.0605	010111	0.7029 -0.1291 + j0.4563 0.0228 – j0.5296
001000	0.4201 0.1033 + j0.5446 -0.6685 – j0.2632	011000	0.387 0.2812 – j0.3980 -0.0077 + j0.7828
001001	0.6591 -0.1405 – j0.6096 0.3407 + j0.2319	011001	0..6658 -0.6858 – j0.0919 0.0666 – j0.2711
001010	0.407 -0.5776 + j0.5744 -0.4133 + j0.0006	011010	0.4436 0.7305 + j0.2507 -0.0580 + j0.4511
001011	0.6659 0.6320 – j0.3939 0.0417 + j0.0157	011011	0.5972 -0.2385 – j0.7188 -0.2493 – j0.0873
001100	0.3550 -0.7412 – j0.0290 -0.3542 + j0.4454	011100	0.5198 0.2157 + j0.7332 0.2877 + j0.2509
001101	0.7173 0.4710 + j0.3756 0.1394 – j0.3211	011101	0.571 0.4513 – j0.3043 -0.5190 –j0.3292
001110	0.3070 -0.0852 – j0.4143 -0.5749 + j0.6295	011110	0.5517 -0.3892 + j0.3011 0.5611 + j0.3724
001111	0.7400 -0.3257 + j0.3461 0.3689 – j0.3007	011111	0.5818 0.1190 + j0.4328 -0.3964 – j0.5504

(cont.)

Matrix index	Column	Matrix index	Column
100000	0.5437 -0.1363 – j0.4648 0.4162 + j0.5446	110000	0.727 -0.5479 – j0.0130 0.3750 – j0.1748
100001	0.5579 -0.6391 + j0.3224 -0.2285 – j0.3523	110001	0.3401 0.4380 + j0.5298 -0.5470 + j0.3356
100010	0.5649 0.6592 – j0.3268 0.1231 + j0.3526	110010	0.6791 -0.1741 – j0.7073 0.0909 – j0.0028
100011	0.484 -0.6914 – j0.3911 -0.3669 + j0.0096	110011	0.3844 -0.1123 + j0.8251 -0.1082 + j0.3836
100100	0.6348 0.5910 + j0.4415 0.2296 – j0.0034	110100	0.6683 0.5567 – j0.3796 -0.2017 – j0.2423
100101	0.4209 0.0760 – j0.5484 -0.7180 + j0.0283	110101	0.394 -0.5255 + j0.3339 0.2176 + j0.6401
100110	0.6833 -0.1769 + j0.4784 0.5208 – j0.0412	110110	0.6976 0.2872 + j0.3740 -0.0927 – j0.5314
100111	0.4149 0.3501 + j0.2162 -0.7772 – j0.2335	110111	0.3819 -0.1507 – j0.3542 0.1342 + j0.8294
101000	0.6726 -0.4225 – j0.2866 0.5061 + j0.1754	111000	0.6922 -0.5051 + j0.2745 0.0904 – j0.4269
101001	0.419 -0.2524 + j0.6679 -0.5320 – j0.1779	111001	0.4083 0.6327 – j0.1488 -0.0942 + j0.6341
101010	0.6547 0.2890 – j0.6562 0.1615 + j0.1765	111010	0.6306 -0.5866 – j0.4869 -0.0583 – j0.1337
101011	0.3843 -0.7637 + j0.3120 -0.3465 + j0.2272	111011	0.4841 0.5572 + j0.5926 0.0898 + j0.3096
101100	0.69 0.6998 + j0.0252 0.0406 – j0.1786	111100	0.5761 0.1868 – j0.6492 -0.4292 – j0.1659
101101	0.3263 -0.4920 – j0.3199 -0.4413 + j0.5954	111101	0.5431 -0.1479 + j0.6238 0.4646 + j0.2796
101110	0.7365 0.0693 + j0.4971 0.2728 – j0.3623	111110	0.5764 0.4156 + j0.1263 -0.4947 – j0.4840
101111	0.3038 0.3052 – j0.2326 -0.6770 + j0.5496	111111	0.549 -0.3963 – j0.1208 0.5426 + j0.4822

APPENDIX 2: PU2RC MULTI-USER SELECTION

PU2RC resource allocation effectively utilizes multi-user precoding and scheduling to enhance MIMO performance. It combines precoder construction and user selection into a single framework. For a system that choose Z users out of M total users, using a codebook with 2^B unitary matrices and P unit vectors in each matrix, the algorithm states

Algorithm 1 MU PU2RC

for $p \in \{1,2,...,P\}$ and $q \in \{1,2,...,2^B\}$ **do**

$$\tilde{z}_{p,q} = \arg\max_{z \in \{1,2,...,M\}} \log(1 + SINR^{z}_{p,q})$$

$$r_{p,q} = \log(1 + SINR^{\tilde{z}}_{p,q})$$

end for

$$(q, \tilde{W}) = \arg\max_{q \in \{1,2,...,2^B\} \times S^Z \in \{1,2,...,P\}} \sum_{p \in Z} r_{p,q}$$

$$\mathbf{W} \leftarrow \tilde{\mathbf{W}} \setminus \{p \in \tilde{\mathbf{W}} : r_{p,q} = 0\}$$

$$z \leftarrow \{\tilde{z}_{p,q}\}_{p \in \mathbf{W}}$$

The *for* loop in Algorithm 1 ensures that each precoding vector in every precoder is only assigned to the user with the highest $SINR$. $\tilde{z}_{p,q}$ represents the user that can achieve the highest sum rate using the $p-th$ column of the $q-th$ in a precoding matrix. $r_{p,q}$ is the corresponding sum rate value. Line 5 of the

algorithm finds the precoder index q and the precoding vectors combination that maximizes Z users' sum rate total. The precoder $\tilde{\mathbf{W}}$ is constructed by stacking the Z precoding vectors in the $q-th$ matrix as row vectors. Line 6 and 7 ensures that user with zero sum rate are not transmitted. i.e. for each user in the selected user set, if its sum rate $r_{p,q}$ is found to be zero, then the user is excluded from the set and the corresponding precoding vector is excluded from the precoding matrix. Note that Algorithm 1 is a modified version of the PU2RC algorithm in [15].

As an example, suppose we have to select 2 users out of a total of 4 users, the codebook contains 4 matrices with 2 columns in each matrix. Let the entries in Table E represents the received SINR values from the 4 mobiles.

Table E SINR CSI (vector 1, vector 2)

	Matrix 1	**Matrix 2**	**Matrix 3**	**Matrix 4**
MS 1	(2,3)	(4,5)	(1,15)	(4,1)
MS 2	(5,2)	(6,1)	(2,5)	(6,1)
MS 3	(7,2)	(1,3)	(20,5)	(4,12)
MS 4	(2,20)	(5,6)	(3,2)	(6,4)

The for loop in the algorithm assigns the user with the maximum sum rate to each precoding vector, which is summarized in Table F.

Table F **User with maximum sum rate for each precoding vector**

	Matrix 1	Matrix 2	Matrix 3	Matrix 4
Vector 1	3	2	3	2
Vector 2	4	4	1	3

Finally, the optimum user pair is selected base on the total sum rate. In this example, the highest total sum rate belongs to matrix 3, where precoding vector 1 assigned to user 3, and precoding vector 2 assigned to user 1 leads to sum rate total of $(\log(1+20)+\log(1+15))$. Therefore, user 1 and user 3 are selected and matrix 3 is used as the precoder.

APPENDIX 3: PUBLICATIONS

At the time of writing, the materials presented in this thesis has been reviewed and accepted by IEEE Conference on Vehicular Technology. The citations are listed here for general reference purpose.

P. Yuan and P. Ho. "Using Direct Analog Feedback for Multiuser MIMO Broadcast Channel," In Proceedings of *IEEE Vehicular Technology Conference, Taiwan, May 16-19, 2010*

P. Yuan and P. Ho. "Hybrid Analog/Digital CSI feedback for Transmit Beamforming Systems in Time-Selective Fading Channels," In Proceedings of *IEEE Vehicular Technology Conference, Taiwan, May 16-19, 2010*

REFERENCE LIST

[1] M. A. Khojastepour, X. Wang, and M. Madihian, "Static and Differential Quantization Codebook Design for MIMO Precoding Systems," in *IEEE GLOBECOM*, 2007, pp. 1592-1596.

[2] W. H. Chin and C. Yuen, "Design of Differential Quantization for Low Bitrates Channel State Information Feedback in MIMO-OFDM Systems," in *IEEE Conference on Vehicular Technology*, 2008, pp. 827-831.

[3] T. Abe and G. Bauch, "Differential Codebook MIMO Precoding Technique," in *IEEE GLOBECOM*, 2007, pp. 3963-3968.

[4] S. Fang, Li L., Q. Cui, and P. Zhang, "Non-Unitary Codebook Based Precoding Scheme for Multi-User MIMO with Limited Feedback,"," in *IEEE Conference on Wireless Communication and Networking*, 2008, pp. 678-682.

[5] K. Amiri, D. Shamsi, B. Aazhang, and J. R. Cavallaro, "Adaptive codebook for beamforming in limited feedback MIMO systems," in *CISS 2008 Annual Conference on Information Sciences and Systems*, 2008, pp. 994-998.

[6] Q. Li and X. Lin, "Compact Feedback for MIMO-OFDM Systems over Frequency Selective Channels," in *IEEE Conference on Vehicular Technology*, Dallas, 2005, pp. 1817-191.

[7] D. J. Love, R. W., Jr. Heath, and T. Strohmer, "Grassmannian beamforming for multiple-input multiple-output wireless systems," *IEEE Transactions on Information Theory*, vol. 49, no. 10, pp. 2735-3747, Oct. 2003.

[8] P. Wu, L. Li, and P. Zhang, "Universal Unitary Space Vector Quantization Codebook Design for Precoding MIMO System under Spatial Correlated Channel," in *IEEE Conference on Vehicular Technology*, 2008, pp. 435-439.

[9] D. J. Love and R. W., Jr. Heath, "Grassmannian beamforming on correlated MIMO channels," in *IEEE GLOBECOM*, 2004, pp. 106-110.

[10] P. Viswanath and D. Tse, "Sum Capacity of the vector Gaussian broadcast channel and uplink-downlink duality," *IEEE Transaction on Information Theory*, vol. 49, no. 8, pp. 1912-1921, Aug. 2003.

[11] M. Costa, "Writing on Dirty Paper," *IEEE Transactions on Information Theory*, vol. 29, no. 3, pp. 439-441, May 1983.

[12] M. Joham, K. Kusume, M. H. Gzara, and W. Utschick, "Transmit Wiener Filter for the Downlilnk of TDD DS-CDMA Systems," in *7th IEEE International Symposium on Spread Spectrum Techniques and Applications*, 2002, pp. 9-13.

[13] X. Shao, J. Yuan, and Y. Shao, "Error Performance analysis of linear zero forcing and MMSE precoder for MIMO broadcast channels," *IEEE IET Communications*, vol. 1, no. 5, pp. 1067-1074, Oct. 2007.

[14] A. D. Dabbagh and D. J. Love, "Multiple Antenna MMSE Based Downlink Precoding with Quantized Feedback or Channel Mismatch," *IEEE Transactions on Communications*, vol. 56, no. 11, pp. 1859-1867, Nov. 2008.

[15] G. Dietl and G. Bauch, "Linear Precoding in the Downlink of Limited Feedback Multiuser MIMO Systems," in *IEEE GLOBECOM*, 2007, pp. 4359-4364.

[16] H. Kim, S. Y. Park, D. J. Love, and S. J. Kim, "Partial Channel State Information Unitary Precoding and Codebook Design for MIMO Broadcast Systems," in *IEEE GLOBECOM*, 2007, pp. 1607-1611.

[17] T. Yoo and A. Goldsmith, "On the Optimality of Multiantenna Broadcast Scheduling Using Zero-Forcing Beamforming," *IEEE Selected Areas in Communications*, vol. 24, no. 3, pp. 528-541, Mar. 2006.

[18] N. Jindal, "MIMO Broadcast Channels With Finite-Rate Feedback," *IEEE Transactions on Information Theory*, vol. 52, no. 11, pp. 5045-5058, Nov. 2006.

[19] M. Edlund, M. Skoglund, and B. D. Rao, "On the Performance of Closed-Loop Transmit Diversity with Non-Ideal Feedback," in *IEEE International Conference on Communications*, 2003, pp. 3190-3194.

[20] K. C. Hwang and K. B. Lee, "Efficient Weight Vector Representation for Closed-Loop Transmit Diversity," *IEEE Transactions on Communications*, vol. 52, no. 1, pp. 9-16, Jan. 2004.

[21] S. Zhou and G. B. Giannakis, "How Accurate Channel Prediction Needs to be for Transmit-Beamforming with Adaptive Modulation over," *IEEE Transactions on Wireless Communications*, vol. 3, no. 4, pp. 1285- 1294, Jul. 2004.

[22] E. Chiu, P. Ho, and J. H. Kim, "Transmit Beamforming with Analog Channel State Information Feedback," *IEEE Transaction on WIreless Communications*, vol. 7, no. 3, pp. 878-889, Mar. 2008.

[23] E. Chiu, "Performance of analog feedback in Closed-loop transmit diversity systems," Simon Fraser University, Vancouver, MaSC Thesis 2006.

[24] "IEEE Standard for Local and Metropolitan Area Networks, Part 16: Air Interface for Fixed and Mobile Broadband Wireless Access," IEEE Std 802.16e,.

[25] Buzo A., Gray R.M. Linde Y., "An algorithm for vector quantizer design," *IEEE Transactions on Communications*, vol. 28, Jan. 1980.

[26] J. G. Proakis, *Digital Communications*, 4th ed. Boston: McGraw-Hill, 2000.

[27] J. H. Conway, R. H. Hardin, and N. J. A. Sloane, "Packing lines, planes, etc.: packing in Grassmannian Spaces," *Experimental Mathematics*, vol. 5, no. 2,

pp. 139-159, Sept. 1996.